iScience

CellPress
OPEN ACCESS

Article

PPT1 regulation of HSP90α depalmitoylation participates in the pathogenesis of hyperandrogenism

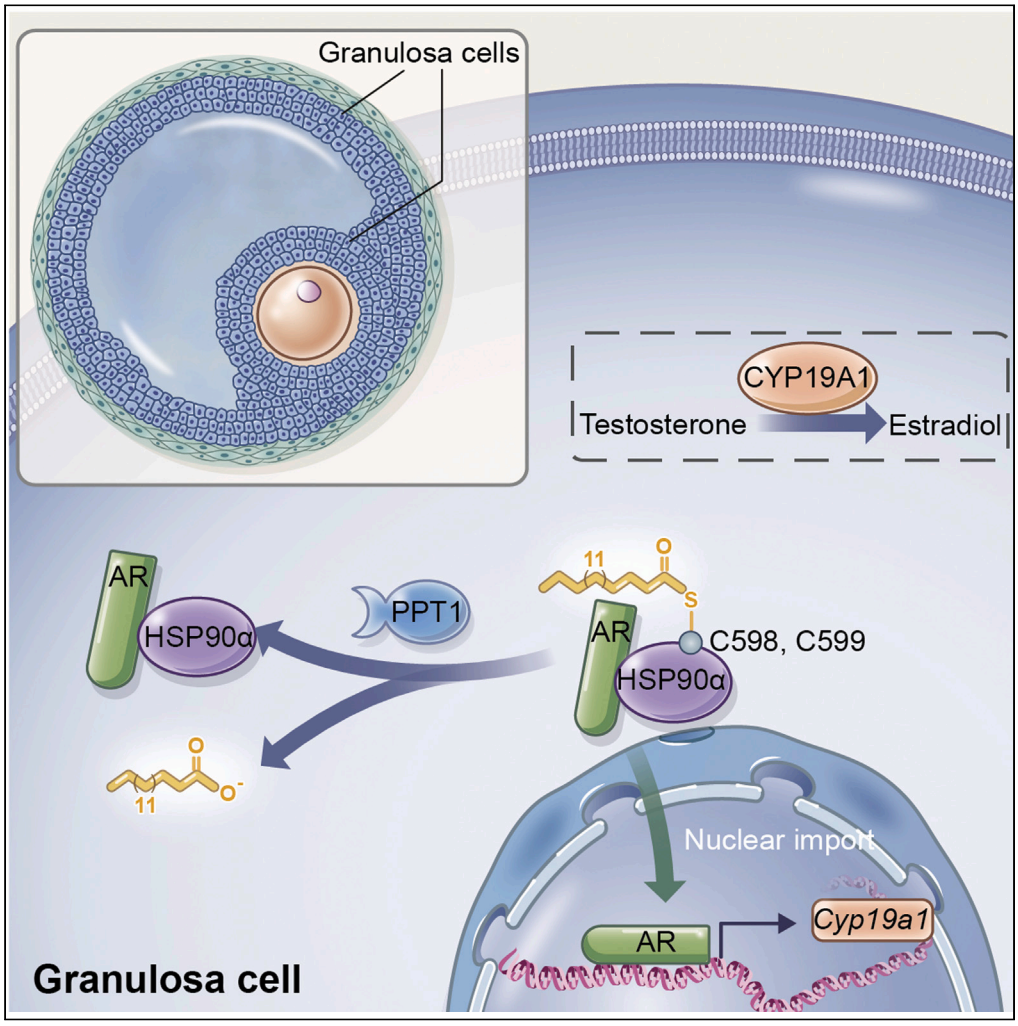

Tongmin Xue, Shanmeizi Zhao, Hong Zhang, ..., Zhigang Guo, Li Chen, Bing Yao

guo@njnu.edu.cn (Z.G.)
yepiaochen@126.com (L.C.)
yaobing@nju.edu.cn (B.Y.)

Highlights

HSP90α *S*-palmitoylation participates in the pathogenesis of hyperandrogenemia

HSP90α-palmitoylation modulates the conversion of androgen to estrogens

HSP90α depalmitoylation could be regulated by PPT1

Dipyridamole attenuated ovarian hyperandrogenism in a DHEA-induced model

Xue et al., iScience *26*, 106131
March 17, 2023
https://doi.org/10.1016/j.isci.2023.106131

iScience

CellPress
OPEN ACCESS

Article

PPT1 regulation of HSP90α depalmitoylation participates in the pathogenesis of hyperandrogenism

Tongmin Xue,[1,4,5,6] Shanmeizi Zhao,[2,3,6] Hong Zhang,[3,6] Ting Tang,[3,6] Lu Zheng,[3,6] Jun Jing,[1,3,4] Xie Ge,[3] Rujun Ma,[3] Jinzhao Ma,[3] Xiaoyan Ren,[2] Kadiliya Jueraitetibaike,[3] Zhigang Guo,[2,*] Li Chen,[1,2,3,4,*] and Bing Yao[1,2,3,4,7,*]

SUMMARY

Ovarian granulosa cells (GCs) in the follicle are the important mediator of steroidogenesis and foster oocyte maturation. Evidences suggested that the function of GCs could be regulated by *S*-palmitoylation. However, the role of *S*-palmitoylation of GCs in ovarian hyperandrogenism remains elusive. Here, we demonstrated that the protein from GCs in ovarian hyperandrogenism phenotype mouse group exhibits lower palmitoylation level compared with that in the control group. Using *S*-palmitoylation-enriched quantitative proteomics, we identified heat shock protein isoform α (HSP90α) with lower *S*-palmitoylation levels in ovarian hyperandrogenism phenotype group. Mechanistically, *S*-palmitoylation of HSP90α modulates the conversion of androgen to estrogens via the androgen receptor (AR) signalling pathway, and its level is regulated by PPT1. Targeting AR signaling by using dipyridamole attenuated ovarian hyperandrogenism symptoms. Our data help elucidate ovarian hyperandrogenism from perspective of protein modification and provide new evidence showing that HSP90α *S*-palmitoylation modification might be a potential pharmacological target for ovarian hyperandrogenism treatment.

INTRODUCTION

The function of ovarian granulosa cells (GCs) is important for female fertility. In female reproductive lifespan, GCs is responsible for steroidogenesis and support oocyte maturation. GCs are primarily responsible for converting thecal androgens to estrogens through the androgen receptor (AR) signaling pathway.[1] Accumulating studies provide evidence that AR signaling dysfunction in GCs is the major pathogenic mechanism for ovarian hyperandrogenism.[2,3]

Ovarian hyperandrogenism can lead to a series of reproductive system disorders and metabolic abnormalities, such as oligo-anovulation, abnormal follicle development, polycystic morphology of the ovary, hyperinsulinemia, and insulin resistance.[4] The use of drugs for treating the symptoms of androgen excess in women has potential adverse effects, including a high risk of intracranial, venous and arterial thrombosis.[5,6] Therefore, a better understanding of the molecular mechanisms of GCs dysfunction and the development of potential therapeutic strategies is critical.

As the barrier of theca cells and oocytes in the follicular environment, GCs are confronted with various physiological stimuli.[7,8] Evidence has suggested that the function of GCs is tightly regulated by post-translational modifications.[9–11] *S*-palmitoylation is a reversible and important post-translational modification on cysteine (Cys) and plays a role in regulating protein functional activity, including protein trafficking, location, stability, protein-protein interactions, and signaling transduction.[12–17] *S*-palmitoylation is dynamically regulated by acyl-transferases (zDHHC domain-containing proteins) and acyl protein thioesterases (for example, APT1, APT2; ABHD family members and palmitoyl-protein thioesterase 1 (PPT1)) to add and remove palmitate, respectively. The key proteins of AR signaling were reported to undergo reversible *S*-palmitoylation, but the function and underlying mechanism remain poorly understood.[18,19] Because of the pivotal role of GCs in female reproductive health, understanding *S*-palmitoylation of GCs-expressed proteins could provide new ways to control ovarian hyperandrogenism.

[1]Reproductive Medical Center, Jinling Hospital Department, Nanjing Medical University, Nanjing, Jiangsu 210002, China

[2]Jiangsu Key Laboratory for Molecular and Medical Biotechnology, College of Life Sciences, Nanjing Normal University, Nanjing, Jiangsu 210023, China

[3]Center of Reproductive Medicine, Nanjing Jinling Hospital, Clinical School of Medical College, Nanjing University, Nanjing, Jiangsu 210002, China

[4]State Key Laboratory of Reproductive Medicine, Nanjing Medical University, Nanjing, Jiangsu 211116, China

[5]Reproductive Medical Center, Clinical Medical College (Northern Jiangsu People's Hospital), Yangzhou University, Yangzhou, Jiangsu 225001, China

[6]These authors contributed equally

[7]Lead contact

*Correspondence: guo@njnu.edu.cn (Z.G.), yepiaochen@126.com (L.C.), yaobing@nju.edu.cn (B.Y.)

https://doi.org/10.1016/j.isci.2023.106131

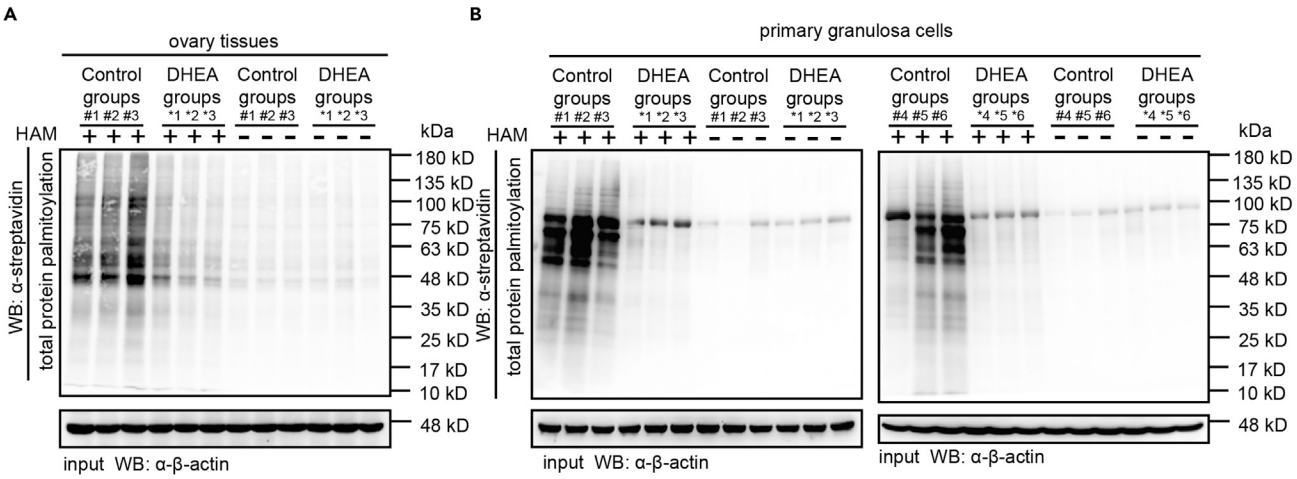

Figure 1. The DHEA-induced ovarian hyperandrogenism mouse model showed lower *S*-palmitoylation modification on GCs-expressed proteins than the control mice

(A) Total protein palmitoylation levels in ovarian tissue in the presence of HAM (1 mM) (n = 3 mice per group).

(B) Primary granulosa cells from the control and DHEA groups were collected to determine the *S*-palmitoylation levels of total protein in the presence of HAM (1 mM) (n = 6 mice per group).

Herein, we identified the property of *S*-palmitoylation of GCs-expressed proteins between dehydroepiandrosterone (DHEA)-induced groups and control groups. We further explored the functional mechanism of downregulated *S*-palmitoylation modified protein, heat shock protein isoform α (HSP90α), in the pathophysiological process of ovarian hyperandrogenism. Mechanistically, (1) *S*-palmitoylation of HSP90α modulates androgen convert to estrogens via DHT-induced AR signaling pathway in GCs; (2) *m*HSP90α undergoes reversible *S*-palmitoylation on Cys598 and Cys599, regulated by PPT1. This finding is consistent with the increased level of PPT1 in patients with ovarian hyperandrogenism. We showed that dipyridamole, a cAMP-elevating phosphodiesterase (PDE) inhibitor, attenuated symptoms of ovarian hyperandrogenism, PCOS, and poor-quality oocytes, in part through activation of AR signaling pathway might via HSP90α *S*-palmitoylation modification.

RESULTS

The DHEA-induced ovarian hyperandrogenism mouse model showed lower *S*-palmitoylation modification than the control mice in ovarian tissue

To validate the role of *S*-palmitoylation in ovarian hyperandrogenism, we established a model of ovarian hyperandrogenism by DHEA-induced mice (Figures S1A–S1K), which are commonly used to study its pathogenesis.[20] To visualize protein *S*-palmitoylation, we applied an ABE assay and found that the global *S*-palmitoylation modification level of proteins in DHEA-induced mouse ovaries was significantly decreased compared with that in the control group (Figure 1A). Owing to the important role of GCs in excess ovarian androgen production, we extracted primary ovarian GCs of individuals from the two groups to further confirm whether the *S*-palmitoylation level of total protein in GCs had the same phenotype as the ovarian tissue presented. The global level of protein palmitoylation in the DHEA group was significantly decreased compared with that in the control group (Figure 1B), suggesting the unique role of *S*-palmitoylation in GCs in the process of ovarian hyperandrogenism.

S-palmitoylation is required for DHT-mediated activation of AR signaling

AR in GCs is known to play a significant role in hyperandrogenism and abnormalities in folliculogenesis.[2,21–23] Before ligand binding, AR exists in a complex with HSP90 and other co-chaperones. There are main steps when AR is activated by binding with androgen, triggering the downstream AR signaling cascade. Initially, the dissociation of AR from the HSP90 complex occurs, followed by a conformational change that facilitates nuclear transport; then, liganded AR interacts with androgen response element (AREs) as a dimer that triggers transcriptional activity of *CYP19A1*, ultimately convert testosterone (TT) to estrogens (E2).[2,24] To determine whether *S*-palmitoylation is required for dihydrotestosterone

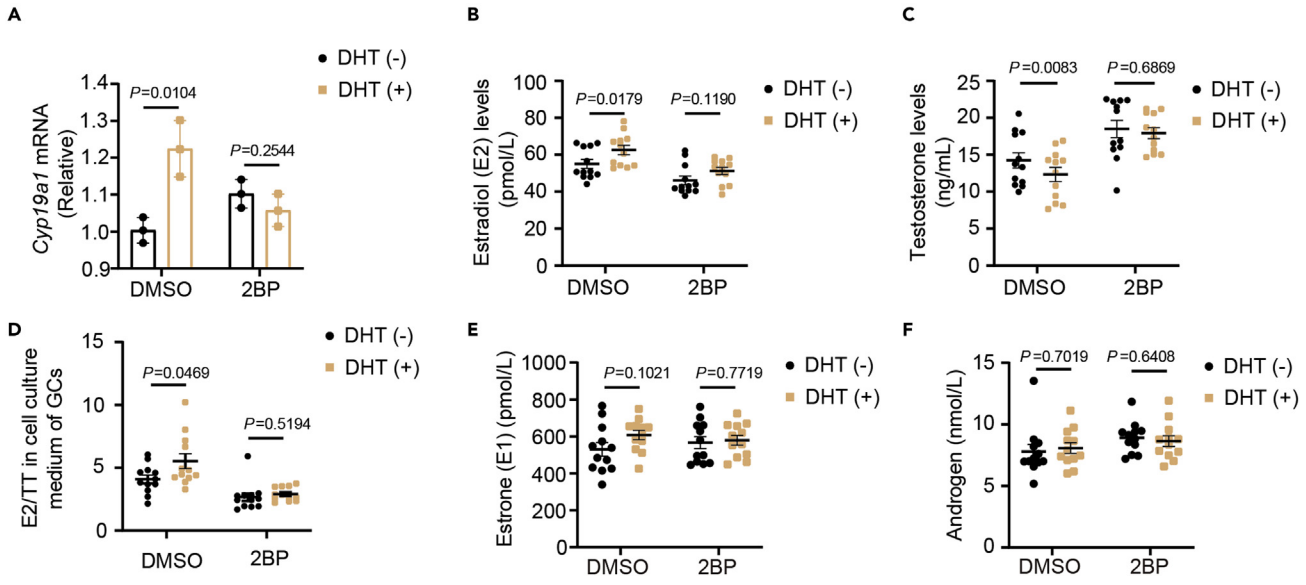

Figure 2. *S*-palmitoylation is required for DHT-induced AR signaling activation

(A) GRM02 cells were treated with 2BP for 24 h and then treated with DHT (100 nM) for 24 h; cell lysates were collected to determine the mRNA level of *Cyp19a1*. GRM02 cells were treated with 2BP (25 μM) for 24h and then treated with DHT (100 nM) for 24 h; cell supernatants were collected to determine the estradiol (B), testosterone (C), estrone (E) and androgen levels (F).

(D) Estrogen to testosterone ratios, analysis based on the data from (B and C) (n = 12). For (B), p values were determined by a two-tailed Mann–Whitney Wilcoxon test, and data are presented as the mean values ± SEM. For (A, C–F), p values were determined by two-tailed Student's *t* test, and data are presented as the mean values ± SEM.

(DHT)-induced AR signaling activation, we treated mouse oocyte granulosa cell line, GRM02 cells with a general *S*-palmitoylation inhibitor, 2-bromopalmitate (2BP), and liganded AR with DHT. The DHT-induced increase in *CYP19A1*-encoding aromatase (Figure 2A) failed in 2BP treatment. In GCs, CYP19A1 is required for estrogens production. We next observed the change of the E2, TT levels and the ratios of E2 to TT in response to DHT-induced AR signal activation. Compared to control groups, palmitoylation inhibitor impaired E2 production, TT consumption, therefore the process TT converts to E2 (Figures 2B–2D), but had little effect on estrone (E1) and androstenedione (ASD) level (FigureFigures 2E and 2F). Taken together, our results indicated that *S*-palmitoylation is required for DHT-mediated AR signaling activation in GCs.

Profiling of palmitoylated proteins in an ovarian hyperandrogenism mouse model

To comprehensively detect the changes in protein palmitoylation in ovarian tissues, we performed an *S*-palmitoylation-enriched quantitative proteomics analysis according to the flowchart shown in Figure 3A. Altogether, we identified 212 proteins from the above samples with a false discovery rate (FDR) less than 1% at both peptide and protein levels. With this approach, a total of 60 palmitoylated proteins were characterized from ovarian tissues between DHEA and control groups (Welch's *t*-test, fold change $\geq$1.2 and p-value $\leq$ 0.05). Widespread *S*-palmitoylation modification was detected on the cysteine residues of the proteins; specifically, and 17 of the proteins (Table S1) exhibited increased levels of *S*-palmitoylation in the DHEA group, and 43 proteins (Table S2) showed decreased levels of *S*-palmitoylation (Figure 3B). Among the 43 identified decreased *S*-palmitoylated proteins in the DHEA groups, the α subtype of heat shock protein 90 (HSP90α, encoded by *Hsp90aa1*), whose *S*-palmitoylation had not been reported, is the key chaperone of androgen receptor, indicating that its *S*-palmitoylation status is highly responsive to ovarian hyperandrogenism in GCs.

HSP90α, a stress-inducible isoform of the molecular chaperone HSP90, has different functions than the constitutively expressed HSP90β isoform.[25] Based on the MS results, we also extracted a representative spectrum for the HSP90α peptide (Figure 3C). *S*-palmitoylation of HSP90α was significantly decreased in the ovaries of the DHEA group compared with the control group (Figure 3D). Notably, no difference in the expression level of HSP90α was found between the control group and the DHEA group by western

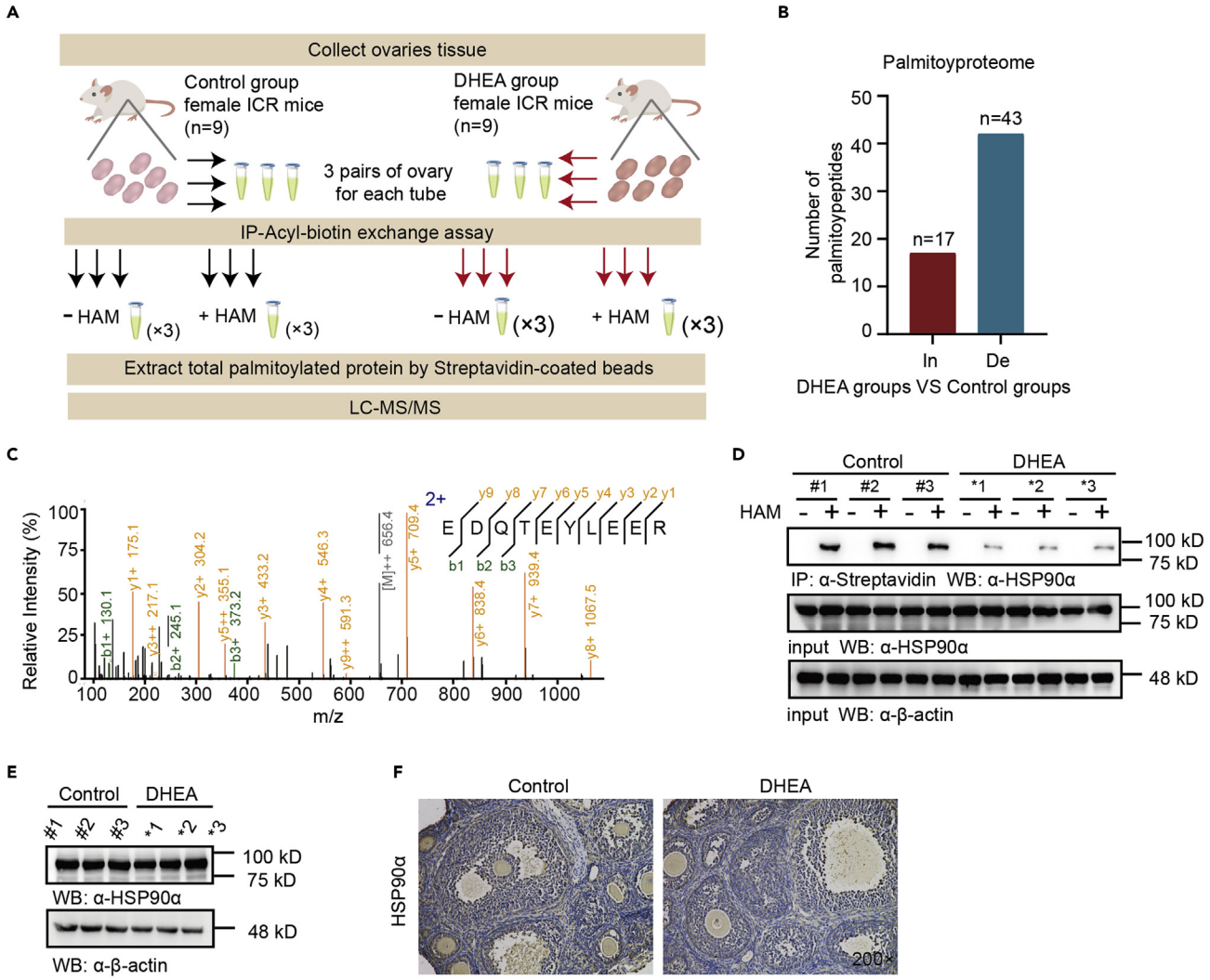

Figure 3. Proteomics reveals *S*-palmitoylated proteins in response to hyperandrogenism

(A) Experimental flowchart for proteomic and *S*-palmitoylation analysis of DHEA and control groups.

(B) Numbers of palmitoyl protein changes in the DHEA and control groups.

(C) Representative spectrum for the HSP90α peptide.

(D) *S*-Palmitoylation levels of HSP90α in mouse ovarian tissue from the control and DHEA groups (n = 3 mice per group) in the presence of HAM (1 mM).

(E) HSP90α expression level in mouse ovarian tissues from the control and DHEA groups (n = 3 mice per group).

(F) Immunohistochemical staining for HSP90α in ovarian tissues; nuclei are shown in blue.

blotting and IHC staining (Figures 3E and 3F). This study thus further focused on exploring the functional mechanism of HSP90α *S*-palmitoylation in the development of ovarian hyperandrogenism.

HSP90α *S*-palmitoylation deficiency impairs AR activation

We implemented a computer program for palmitoylation site prediction, the Clustering and Scoring Strategy for Palmitoylation Sites Prediction (CSS-Palm) system, and found potential palmitoylation sites at Cys^{598}/Cys^{599} of the *m*HSP90α protein, which are homologous to Cys^{597}/Cys^{598} of the *h*HSP90α protein. Sequence alignment of the HSP90α protein at Cys^{598}/Cys^{599} between different species showed that *m*HSP90α's palmitoylation sites had a high degree of homology between species (Figure 4A), and the ribbon representation of the S-palmitoylation sites on a *m*HSP90α 3D structure model is shown in Figure 4B.

To unveil the roles of HSP90α palmitoylation, we generated an *m*HSP90α mutant in which Cys^{598} and/or Cys^{599} was mutated to Ser (*m*HSP90α^{C598S}, *m*HSP90α^{C599S}, and *m*HSP90α^{C598,599S}) and then expressed

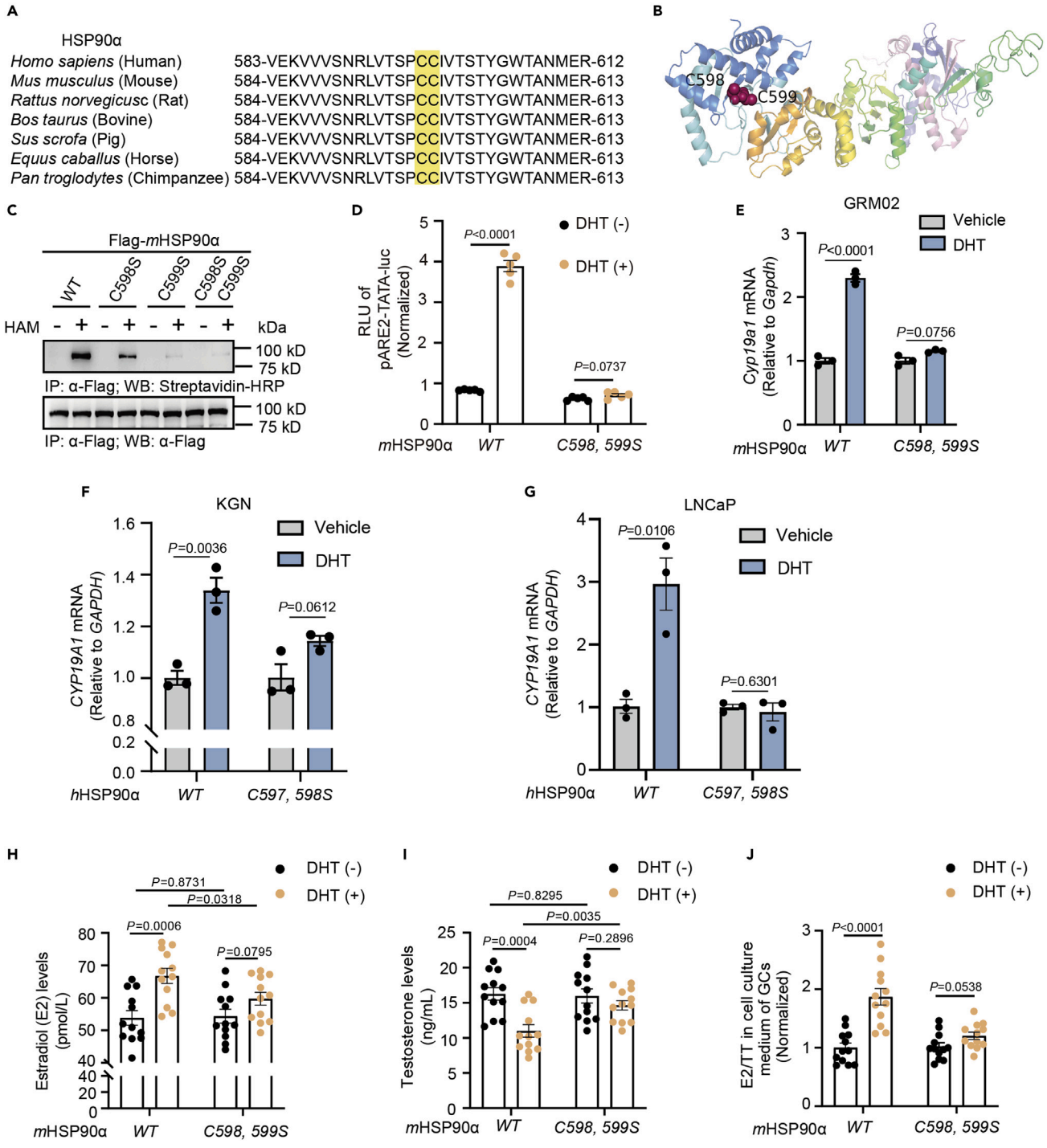

Figure 4. HSP90α *S*-palmitoylation deficiency impairs DHT-induced AR activation

(A) Alignment of HSP90α protein sequences among different species.

(B) Ribbon representation of the *S*-palmitoylation sites on a *m*HSP90α 3D structure model. (Single-letter abbreviations for the amino acid residue: C, cysteine).

(C) Palmitoylation levels of Flag-tagged wild-type (WT) *m*HSP90α or *m*HSP90α (C598S), *m*HSP90α (C599S) and *m*HSP90α (C598S, C599S).

(D) DHT-induced transcriptional activation of a classic ARE-luciferase reporter in HEK293T cells (n = 5) transiently transfected with Flag-*m*HSP90α^{WT} or *S*-palmitoylation-deficient Flag-*m*HSP90α$^{C598,\ 599S}$. The data are presented as the means ± SEMs, and p values were determined by unpaired two-tailed Student's *t* tests of n = 5 independent biological experiments.

Figure 4. *Continued*

(E) The GRM02 cells were transfected with Flag-*m*HSP90α^{WT} or Flag-*m*HSP90α$^{C598,\ 599S}$ and then treated with DHT (100 nM) for 24h. Cell lysates were collected to determine the mRNA level of *Cyp19a1*.

(F and G) The KGN and LNCaP cells were transfected with Flag-*h*HSP90α^{WT} or Flag-*h*HSP90α$^{C597,\ 598S}$ and then treated with DHT (10 nM) for 24h. Cell lysates were collected to determine the mRNA level of *CYP19A1*. Estradiol (H) and testosterone (I) levels in the supernatants of GRM02 cells (n = 12) transiently transfected with Flag-WT *m*HSP90α or *S*-palmitoylation-deficient Flag-*m*HSP90α$^{C598,\ 599S}$ after stimulation with DHT (100 nM) for 24h, as measured by ELISA.

(J) Estradiol to testosterone ratios, using the data from (H) and (I) (n = 12). In (D–F), all error bars, mean values ±SEM, and p values were calculated using unpaired two-tailed Student's *t* tests.

mutant or wild-type HSP90α (*m*HSP90α^{WT}) in 293T cells. These single- or double-cysteine HSP90α mutants exhibited decreased palmitoylation levels, and palmitoylation of the HSP90α double-Cys mutant was further reduced by more than 75% compared with that of the HSP90α mono-Cys mutants (Figure 4C). DHT-induced transcriptional activation of a classic ARE-luciferase reporter in HEK293T cells transiently transfected with *S*-palmitoylation-deficient Flag-*m*HSP90α^{C598,599S} indicated that AR agonist ARE-dependent luciferase activity could not be induced (Figure 4D). Furthermore, in response to DHT stimulation, the HSP90α *S*-palmitoylation-deficient mutant decreased the transcriptional activity of *CYP19A1* compared with HSP90α^{WT} in GRM02, KGN, and LNCaP cells (Figures 4E–4G). Accordingly, GRM02 expressing Flag-*m*HSP90α^{C598,599S} failed to increase the ratios of E2 to TT (Figures 4H–4J). The HSP90α equal protein expression between WT and mutants were shown in Figure S2. Thus, *S*-palmitoylation of HSP90α is required for DHT-induced AR activation and altered steroidogenesis.

PPT1 catalyses the depalmitoylation of HSP90α

We aimed to identify the enzyme that might catalyze depalmitoylation of HSP90α and found that all the palmitoylation signals of HSP90α were decreased after co-expression the well-known acyl protein thioesterases compared with control group. We focused on PPT1, which showed the strongest effect in depalmitoylating HPS90α (Figure 5A) and confirmed endogenous PPT1 interacts with endogenous HSP90α (Figure 5B). PPT1 is generally considered to be a lysosomal enzyme, and HSP90α is reported mainly expressed cytosol.[26–29] To investigate the distribution of HSP90α and PPT1, we conducted the subcellular fractionation experiment and observed that HSP90α and PPT1 are both detected in the lysosome enriched component (Figure 5C). To probe the potential role of PPT1 for ovarian hyperandrogenism, we detected the expression of PPT1 in the DHEA group and control group. In mouse ovarian biopsies, PPT1 expression was elevated in the DHEA-treated mice compared with the control group (Figure 5D). These results suggest that changes in the expression of PPT1 might be more relevant for ovarian hyperandrogenism. To determine the clinical value of the observed PPT1-regulated *S*-palmitoylation in ovarian hyperandrogenism, we performed IHC analysis of ovarian samples from six patients with ovarian hyperandrogenism and five patients without ovarian hyperandrogenism (Table S3) with anti-PPT1. PPT1 was higher expressed in ovarian samples from six patients with ovarian hyperandrogenism compared to the control group (Figures 5E–5G). Taken together, these analyses reveal that a high level of PPT1 expression correlates with the clinical development of ovarian hyperandrogenism.

PPT1 depalmitoylates HSP90α and abolishes DHT-induced AR activation

To further study the function of PPT1, we overexpressed HA-tagged PPT1 or HA-tagged EV in GRM02 cells, as confirmed by using Western blotting; the results showed that when transfected with HA-tagged PPT1, endogenous HSP90α was clearly de-palmitoylated (Figure 6A). These results indicate that PPT1 depalmitoylates HSP90α. To confirm whether PPT1 is an endogenous HSP90α depalmitoylase, we generated GRM02 cell lysates pulldown endogenous HSP90α and divided them into two fractions, one of which was identified by using immunoprecipitation (Figure 5B), whereas the other was used for MS. Then, based on the MS results, we also extracted a representative spectrum for the PPT1 peptide (Figure 6B). Accordingly, GRM02 expression of *Cyp19a1* significantly decreased after transfection with HA-PPT1 (Figure 6C) and failed to increase the ratios of E2 to TT (Figures 6D–6F). However, transfection with HA-PPT1 did not affect the ratios of E1 to ASD (Figures 6G and 6H). Collectively, the data support the hypothesis that PPT1 preferentially promotes HSP90α depalmitoylation and that this modification is required for *Cyp19a1*-encoded aromatase and altered GRM02 steroidogenesis.

Dipyridamole supplementation alleviates ovarian hyperandrogenism-like symptoms and regulates HSP90α S-palmitoylation

Thus far, we have shown that ovarian hyperandrogenism is characterized by low palmitoylated modification protein in GCs, and defective AR signaling activation may function as a common mechanism. Several

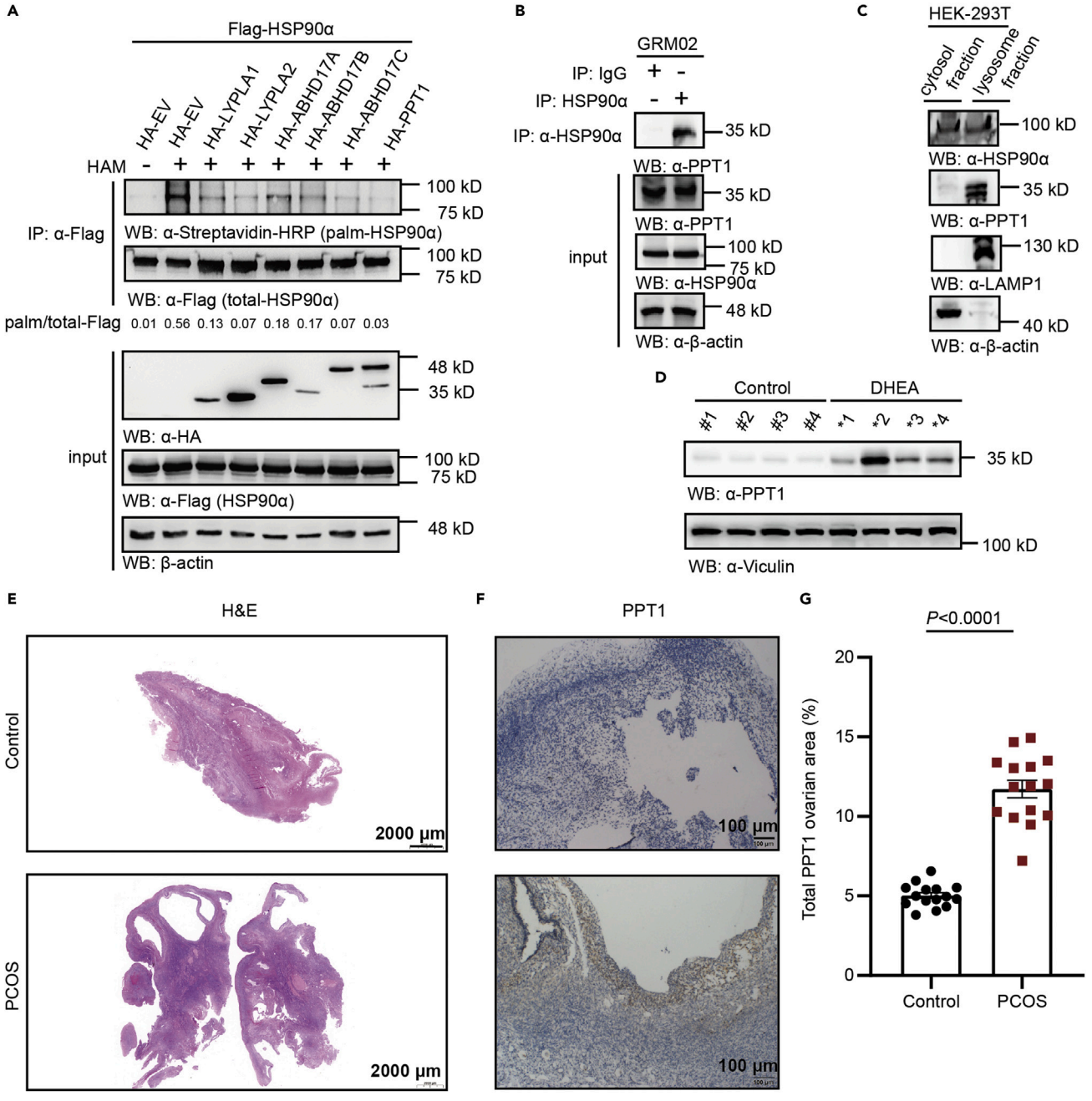

Figure 5. PPT1 catalyses the depalmitoylation of HSP90α

(A) HEK293T cells were transfected with plasmids coding Flag-HSP90α together with HA-tagged empty vector, HA-tagged LYPLA1, HA-tagged LYPLA2, HA-tagged ABHD17A, HA-tagged ABHD17B, HA-tagged ABHD17C or HA-tagged PPT1 and plasmid to screen for thioesterases that could decrease HSP90α palmitoylation. For (A), the palmitoylation level was detected using the ABE method.

(B) Endogenous PPT1 interacts with endogenous HSP90α in GRM02 cells.

(C) Endogenous HSP90α was detected in lysosome-enriched fraction.

(D) PPT1 expression levels in mouse ovarian tissues from the control and DHEA groups (n = 4 mice per group).

(E) Representative hematoxylin-eosin (H&E)-stained sections from the ovaries of the control and ovarian hyperandrogenism groups. Scale bar: 2000 μm.

(F) Immunohistochemical staining with PPT1 in ovarian tissues; nuclei in blue. Scale bar: 100 μm.

(G) Quantitative analysis of the positive area per field by ImageJ software (NIH) with ImmunoRatio Plugin. The data are presented as the means of three fields and expressed as the means ± SDs (n = 5).

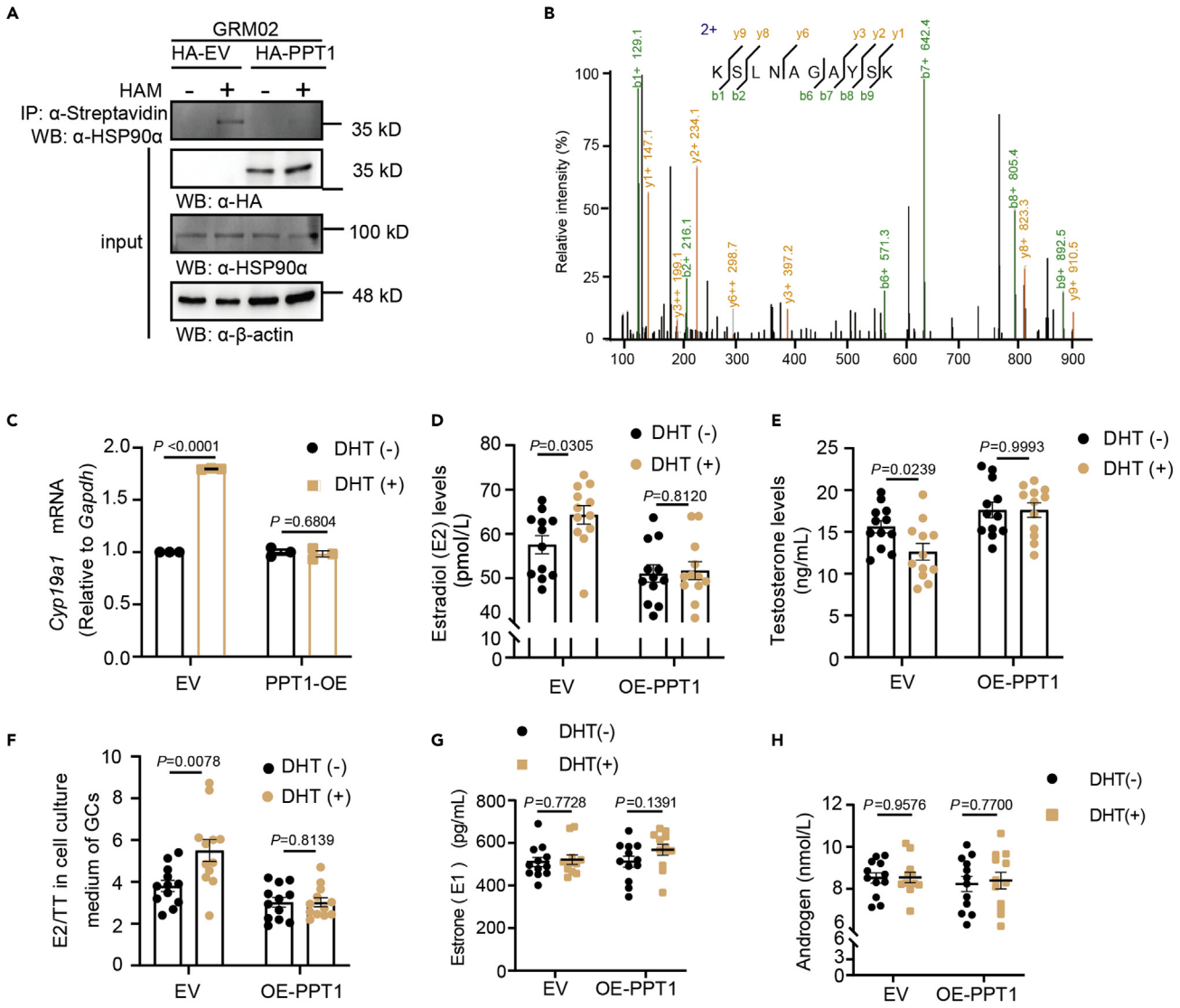

Figure 6. PPT1 depalmitoylates HSP90α and abolishes DHT-induced AR activation

(A) Endogenous HSP90α palmitoylation levels after transfection with HA-tagged empty vector or HA-tagged PPT1 in GRM02 cells.

(B) Representative spectrum for the HSP90α peptide.

(C) GRM02 cells were transfected with HA-tagged PPT1 and then treated with DHT (100 nM) for 24h. Cell lysates were collected to determine the mRNA level of *Cyp19a1*. Cell supernatants were collected to determine the estradiol (D), testosterone (E) levels, the estrone (G) and androgen levels (H). (F) Estradiol to testosterone ratios; analysis based on the data from (D) and (E) (n = 12). For (D, E, and H), p values were determined by two-tailed Student's *t* test, and data are presented as the mean value ± SEM. For (G), p values were determined by a two-tailed Mann–Whitney Wilcoxon test, and data are presented as the mean values ± SEM.

studies have demonstrated that AR can be stimulated by high cAMP levels.[30,31] Therefore, we determined whether targeting AR signaling activation *in vivo* with dipyridamole, a cAMP-elevating PDE inhibitor, could reverse ovarian hyperandrogenism. Dipyridamole treatment recovered ovarian morphology, the estrous cycle, and the hormone profile compared with those of the mice treated with DHEA alone (Figures 7A–7F).

Patients with ovarian hyperandrogenism in PCOS have a lower quality of oocyte and embryo development those without PCOS in assisted reproductive technology.[32] The quality of oocyte and oocyte maturation was assessed by the GVBD rate and the first polar body extrusion (PBE) rate, respectively. In a DHEA-induced model, we found that the GVBD rate and the PBE rate from mice orally gavage with

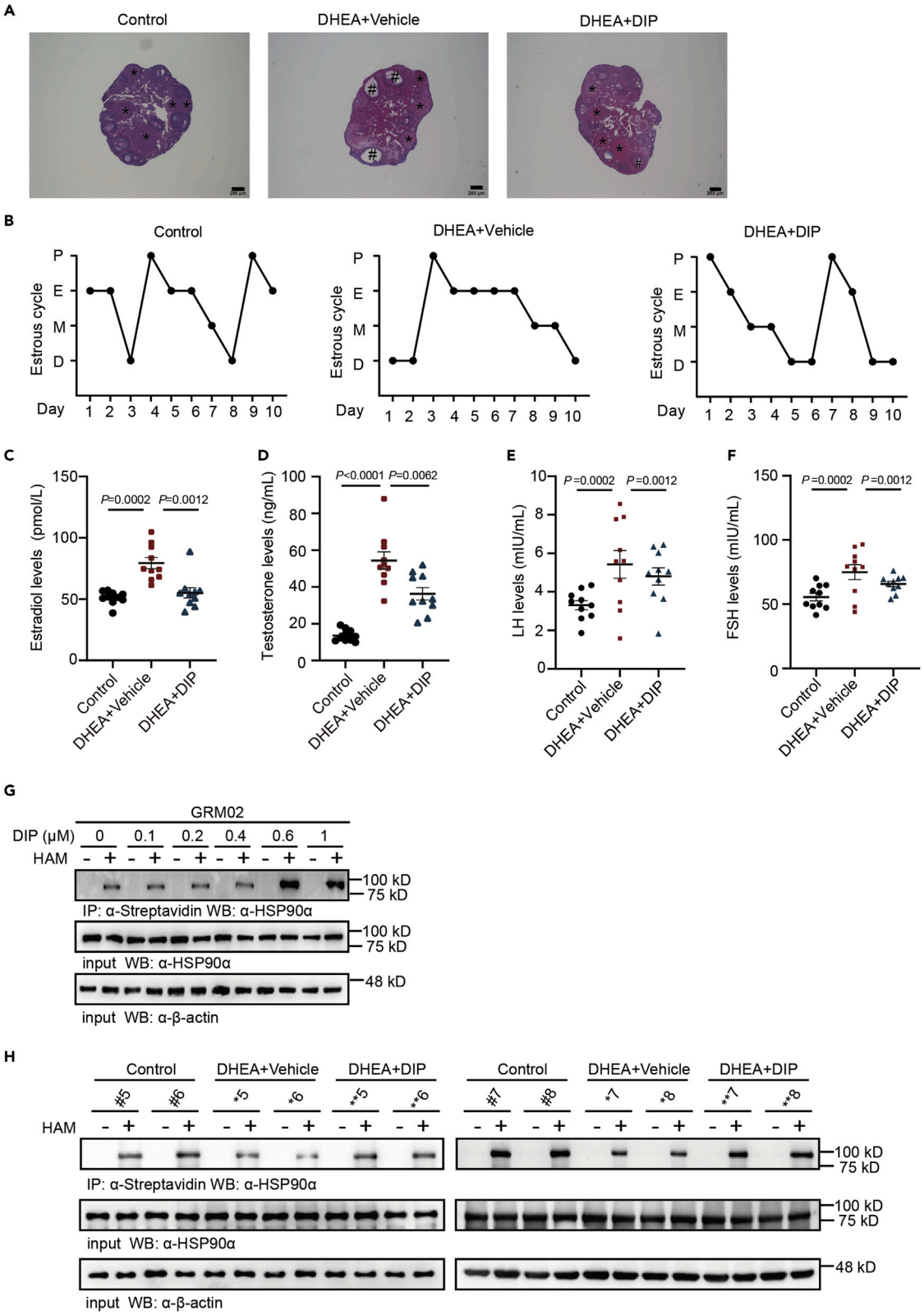
A
Control
DHEA+Vehicle
DHEA+DIP
B
Control
DHEA+Vehicle
DHEA+DIP
Estrous cycle
P
E
M
D
Day
1 2 3 4 5 6 7 8 9 10
C
Estradiol levels (pmol/L)
P=0.0002
P=0.0012
D
Testosterone levels (ng/mL)
P<0.0001
P=0.0062
E
LH levels (mIU/mL)
P=0.0002
P=0.0012
F
FSH levels (mIU/mL)
P=0.0002
P=0.0012
Control
DHEA+Vehicle
DHEA+DIP
G
GRM02
DIP (μM) 0 0.1 0.2 0.4 0.6 1
HAM - + - + - + - + - + - +
100 kD
75 kD
IP: α-Streptavidin WB: α-HSP90α
input WB: α-HSP90α
48 kD
input WB: α-β-actin
H
Control
DHEA+Vehicle
DHEA+DIP
#5 #6 *5 *6 **5 **6
#7 #8 *7 *8 **7 **8
HAM
IP: α-Streptavidin WB: α-HSP90α
input WB: α-HSP90α
input WB: α-β-actin

Figure 7. Dipyridamole supplementation alleviates DHEA-induced hyperandrogenism symptoms and regulates HSP90α palmitoylation

(A) Representative hematoxylin-eosin (H&E)-stained sections from the ovaries of the control, DHEA, and DHEA + dipyridamole (DIP) groups. Scale bar: 200 μm. The asterisk (*) represents the corpus luteum, and the pound sign (#) represents the ovary vacuoles.

(B) Representative estrous cycles.

(C) Serum estradiol levels in the control (black plots), DHEA (red plots), and DHEA + DIP (blue plots) groups (n = 10 mice per group).

(D) Testosterone levels in the serum of the control (black plots), DHEA (red plots), and DHEA + DIP (blue plots) groups (n = 10 mice per group).

(E) LH levels in the serum of the control (black plots), DHEA (red plots), and DHEA + DIP (blue plots) groups (n = 10 mice per group).

(F) FSH levels in the serum of the control (black plots), DHEA (red plots), and DHEA + DIP (blue plots) groups (n = 10 mice per group).

(G) Endogenous HSP90α palmitoylation levels were detected with the indicated concentration of DIP treatment for 4h in the presence of HAM.

(H) HSP90α palmitoylation levels were detected in mouse ovarian tissues from the control, DHEA, and DHEA + DIP groups (n = 4 mice per group) in the presence of HAM. For (C, E and F), p values were determined by a two-tailed Mann–Whitney Wilcoxon test, and the data are presented as the mean values ± SEMs. For (D), p values were determined by two-tailed Student's *t* test, and the data are presented as the mean values ± SEMs.

dipyridamole increased (Figures S3A–S3D). These results suggest that dipyridamole can effectively improve the maturation ability of DHEA-treated oocytes.

DHT-mediated activation of AR signaling was largely impeded because of HSP90α's *S*-palmitoylation modification. We next investigated whether dipyridamole supplementation could reverse HSP90α hypo-palmitoylation level in the DHEA groups. First, we treated GRM02 cells with different concentrations of dipyridamole, and the levels of HSP90α palmitoylation significantly increased with 0.6 μM dipyridamole, suggesting that the compound could increase HSP90α palmitoylation *in vitro* (Figure 7G). To confirm the level of *S*-palmitoylated HSP90α, we found that HSP90α palmitoylation was significantly higher in the DHEA + dipyridamole group than in the DHEA group (Figure 7H). These data indicate that dipyridamole recovered ovarian dysfunction may through increased HSP90α palmitoylation in the ovarian hyperandrogenism phenotype model.

DISCUSSION

We present evidence that DHT-mediated activation of AR signaling is modulated by HSP90α *S*-palmitoylation modification in GCs contributing to the ovarian hyperandrogenism pathological process. That these mouse studies have applicability to human disease is supported by our data establishing PPT1 expression tendencies in patients' ovary tissues. Together, our data support the conclusion that HSP90α *S*-palmitoylation modification might be a tractable pharmacological target for the treatment of PCOS.

It is important to note that dipyridamole could improve HSP90α *S*-palmitoylation modification in mouse *in vivo* and *in vitro* experiments. As a platelet function inhibitor, dipyridamole was introduced on the market as a coronary vasodilator drug more than half a century ago and is still used as an antithrombotic and vasodilator.[33] Oral contraceptives (OCPs), the regular approved drug for treating symptoms of androgen excess in women with PCOS, have potential adverse effects.An international multicentre case-control study reported that oral OCPs are associated with an increased risk for venous thromboembolism.[34] There is relatively strong evidence suggesting that PCOS is associated with increased platelet aggregation and decreased plasma fibrinolytic activity.[35] From the anti-androgens and prevent thrombosis, treatment for androgen excess in patients with high risk in thromboembolism could consider dipyridamole as a complementary or alternative drug. Moreover, it should be emphasized that PCOS is a heterogeneous endocrine condition, and drugs for treating symptoms of PCOS should be under comprehensive consideration. In the future, the effect of dipyridamole targeting androgen excess in PCOS patients will need placebo-controlled trial validation.

Ovarian hyperandrogenism and insulin resistance are the main causes of PCOS, and they can interact with each other in the occurrence and development of PCOS.[36–38] In our study, in comparison with the control groups, 43 protein *S*-palmitoylation levels were decreased in the DHEA-induced groups (Figure 1C). Notably, we observed that insulin receptor-related proteins (IRR, Entry: Q9 WTL4) were included. A previous report showed that IRR inactivation impedes insulin signaling by blocking phosphorylation of the primary adaptor insulin receptor substrate-1 (IRS-1).[39] We envision that the S-polarization alteration of IRR might impede its activation by remodeling the structure of the cysteine-rich domain.[40] Considering these findings, the *S*-palmitoylation modification of IRR may be a mechanism underlying the contribution of hyperandrogenism to insulin resistance in PCOS. Our data in ovary tissue demonstrate a notable association of decreased *S*-palmitoylation and PCOS, which strongly supports ovarian hyperandrogenism and ovulation symptoms in PCOS.

Studies in the past few years have focused on abnormal AR, and AR dysfunction in GCs is associated with PCOS.[2,41,42] AR is chaperoned by HSP90 in the cytosol.[24] In this study, we proved that DHT-induced AR activation is modulated by HSP90α *S*-palmitoylation modification. We used an *in vitro* cell line model to show that downstream of DHT-induced AR activation, HSP90α *S*-palmitoylation was impaired by HSP90α$^{C598,\ 599S}$ inhibition or PPT1 overexpression. Our data showed that HSP90α *S*-palmitoylation in the ovarian environment was associated with ovarian hyperandrogenism. Future studies might determine whether PPT1 is inducibly expressed under excess androgen conditions, perhaps because hyperandrogenism and palmitoylation are a vicious cycle.

In mammalian cells, although HSP90 has two main isoforms, α and β, alpha is an inducible isoform that responds to stress. Previous reports about HSP90 chaperone function in steroid receptors have not distinguished which isoform has a greater contribution and whether *S*-palmitoylation modification of HSP90α impacts AR activation.[43] In support of our finding, DDO-66000, a covalent modification of Cys598 on *h*HSP90α, has been reported previously, showing that it blocks HSP90-CDC37, which plays a role in chaperone function.[44] Combining this report and our data suggests that HSP90α contributes more to DHT-induced AR activation than HSP90β. Although HSP90α is highly expressed in the cytoplasm and PPT1 is highly expressed in lysosome, HSP90α were detected in the lysosome enriched component (Figure 5C). These differences hint toward a possible mechanism of HSP90α de-palmitoylated by PPT1 occurred in lysosome.

From the molecular biology view, many types of PTMs have been reported on HSP90α, including phosphorylation and S-nitrosylation.[45–47] A new PTM on HSP90α was reported in our study, showing that the *S*-palmitoylation modification level of the specific α isoform of HSP90 modulates the DHT-induced AR signaling pathway activation. AR activation is also involved in the development and progression of prostate cancer, which is one of the most frequently diagnosed cancers in males.[48] Based on our findings (Figure 4G), it is suggested that hindering AR activation by *S*-palmitoylation modification could be useful in the treatment of prostate cancer. AR is a member of a steroid receptor superfamily that includes the glucocorticoid receptor, mineralocorticoid receptor, estrogenic receptor α/β, and progesterone receptor A/B. Steroid receptor superfamily members are important clients for HSP90.[49] Whether HSP90α palmitoylation interferes with other members of the steroid receptor superfamily is an interesting issue.

In the present study, we present a comparative profile of protein *S*-palmitoylation in ovary tissue from DHEA-treated hyperandrogenism phenotype group. We further investigated the functional mechanism by which HSP90α *S*-palmitoylation modulates androgen conversion to estrogens via AR signaling pathway in GCs, contributing to the pathophysiological process of ovarian hyperandrogenism. In detail, *m*HSP90α undergoes reversible *S*-palmitoylation on Cys598 and Cys599, and its palmitoylation level could be regulated by PPT1 (Figure 8). This finding is consistent with the increased level of PPT1 in individuals with hyperandrogenism. As such, we proposed that targeting *S*-palmitoylation is a plausible approach to treat hyperandrogenism. From the therapeutic strategy to ameliorate AR inactivation, we tested dipyridamole, a PDE inhibitor with a good safety record and wide availability, attenuated ovarian hyperandrogenism, which was mediated, at least in part, by elevated *S*-palmitoylated HSP90α.

Limitations of the study

There are some limitations to this study: (1) The LC-MS/MS spectrum of the *S*-palmitoylation modified peptide comprising residues Cys598 and Cys599 of *m*HSP90α is lacking. (2) *S*-palmitoylated HSP90α alterations have not been verified under pathological conditions from GCs of PCOS patients.

STAR★METHODS

Detailed methods are provided in the online version of this paper and include the following:

- KEY RESOURCES TABLE
- RESOURCE AVAILABILITY
  - Lead contact
  - Materials availability
  - Data and code availability
- EXPERIMENTAL MODEL AND SUBJECT DETAILS
  - Mice

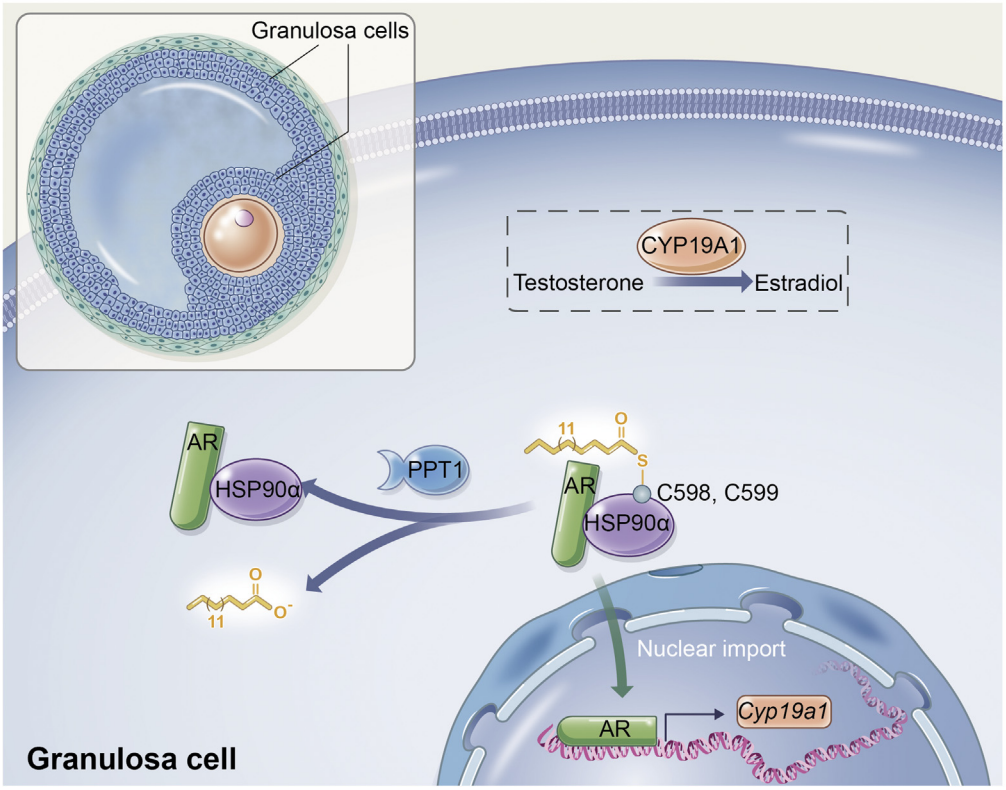

Figure 8. Schematic of hypotheses concerning the mechanisms underlying the role of palmitoylation of HSP90α in regulating hyperandrogenism in PCOS

- Cell lines
- Isolation of primary mouse granulosa cells

- METHOD DETAILS
  - The dehydroepiandrosterone (DHEA)-induced hyperandrogenism phenotype mouse model
  - Vaginal smears and oestrous cycle determination
  - Serum analysis
  - Human tissue specimens
  - Morphology and immunohistochemistry
  - Acyl-biotin exchange (ABE)-based sample preparation for mass spectrometry
- QUANTIFICATION AND STATISTICAL ANALYSIS

SUPPLEMENTAL INFORMATION

Supplemental information can be found online at https://doi.org/10.1016/j.isci.2023.106131.

ACKNOWLEDGMENTS

This work was supported by the National Key Research and Development Program of China (grant nos. 2018YFC1004700), the Medical Scientific Research Key Project of Jiangsu Commission of Health (ZD2022004) and the National Natural Science Foundation of China (grants 81701431, 82271687, 81872284, 32000583, 81973965, 82274651). We sincerely thank Prof. Ling Lu from Nanjing Normal University for her kind help with our palmitoylated protein analysis experiments. We thank Yao Xu, Kemei Zhang and Weiqing Chen for their assistance in lysosome isolation and serum analysis assay. We also thank the other members of Prof. Yao's laboratory for their discussion and insights.

AUTHOR CONTRIBUTIONS

Conceptualization: B.Y., and L.C.; Methodology: T.X., S.Z., X.G., R.M., J.J., J.M., and K.J.; Investigation: T.X., S.Z., T.T., L.Z., H.Z., and X.R.; Data Analysis: S.Z., H.Z., and L.Z.; Visualization: S.Z.; Writing – Original Draft: S.Z.; Writing – Review and Editing: S.Z.; Supervision: B.Y., L.C., and Z.G.; Funding Acquisition: B.Y., L.C., Z.G., J.J., R.M., and K.J.

DECLARATION OF INTERESTS

The authors declare no competing interests.

Received: September 21, 2022
Revised: November 9, 2022
Accepted: January 31, 2023
Published: February 3, 2023

REFERENCES

1. Mason, H.D., Willis, D.S., Beard, R.W., Winston, R.M., Margara, R., and Franks, S. (1994). Estradiol production by granulosa cells of normal and polycystic ovaries: relationship to menstrual cycle history and concentrations of gonadotropins and sex steroids in follicular fluid. J. Clin. Endocrinol. Metab. *79*, 1355–1360. https://doi.org/10.1210/jcem.79.5.7962330.

2. Wang, F., Pan, J., Liu, Y., Meng, Q., Lv, P., Qu, F., Ding, G.L., Klausen, C., Leung, P.C.K., Chan, H.C., et al. (2015). Alternative splicing of the androgen receptor in polycystic ovary syndrome. Proc. Natl. Acad. Sci. USA *112*, 4743–4748. https://doi.org/10.1073/pnas.1418216112.

3. McFee, R.M., Romereim, S.M., Snider, A.P., Summers, A.F., Pohlmeier, W.E., Kurz, S.G., Cushman, R.A., Davis, J.S., Wood, J.R., and Cupp, A.S. (2021). A high-androgen microenvironment inhibits granulosa cell proliferation and alters cell identity. Mol. Cell. Endocrinol. *531*, 111288. https://doi.org/10.1016/j.mce.2021.111288.

4. Rodriguez Paris, V., and Bertoldo, M.J. (2019). The mechanism of androgen actions in PCOS etiology. Med. Sci. *7*, 89.

5. Weill, A., Nguyen, P., Labidi, M., Cadier, B., Passeri, T., Duranteau, L., Bernat, A.L., Yoldjian, I., Fontanel, S., Froelich, S., and Coste, J. (2021). Use of high dose cyproterone acetate and risk of intracranial meningioma in women: cohort study. BMJ *372*, n37. https://doi.org/10.1136/bmj.n37.

6. Wu, C.Q., Grandi, S.M., Filion, K.B., Abenhaim, H.A., Joseph, L., and Eisenberg, M.J. (2013). Drospirenone-containing oral contraceptive pills and the risk of venous and arterial thrombosis: a systematic review. BJOG *120*, 801–810. https://doi.org/10.1111/1471-0528.12210.

7. Xu, L., Wang, W., Zhang, X., Ke, H., Qin, Y., You, L., Li, W., Lu, G., Chan, W.Y., Leung, P.C.K., et al. (2019). Palmitic acid causes insulin resistance in granulosa cells via activation of JNK. J. Mol. Endocrinol. *62*, 197–206. https://doi.org/10.1530/jme-18-0214.

8. Chen, Z., Lei, L., Wen, D., and Yang, L. (2019). Melatonin attenuates palmitic acid-induced mouse granulosa cells apoptosis via endoplasmic reticulum stress. J. Ovarian Res. *12*, 43. https://doi.org/10.1186/s13048-019-0519-z.

9. Rodriguez, A., Briley, S.M., Patton, B.K., Tripurani, S.K., Rajapakshe, K., Coarfa, C., Rajkovic, A., Andrieux, A., Dejean, A., and Pangas, S.A. (2019). Loss of the E2 SUMO-conjugating enzyme Ube2i in oocytes during ovarian folliculogenesis causes infertility in mice. Development *146*, dev176701. https://doi.org/10.1242/dev.176701.

10. Uzbekova, S., Teixeira-Gomes, A.-P., Marestaing, A., Jarrier-Gaillard, P., Papillier, P., Shedova, E.N., Singina, G.N., Uzbekov, R., and Labas, V. (2021). Protein palmitoylation in bovine ovarian follicle. Int. J. Mol. Sci. *22*, 11757. https://doi.org/10.3390/ijms222111757.

11. Min, Z., Long, X., Zhao, H., Zhen, X., Li, R., Li, M., Fan, Y., Yu, Y., Zhao, Y., and Qiao, J. (2020). Protein lysine acetylation in ovarian granulosa cells affects metabolic homeostasis and clinical presentations of women with polycystic ovary syndrome. Front. Cell Dev. Biol. *8*, 567028. https://doi.org/10.3389/fcell.2020.567028.

12. Zhang, M., Zhou, L., Xu, Y., Yang, M., Xu, Y., Komaniecki, G.P., Kosciuk, T., Chen, X., Lu, X., Zou, X., et al. (2020). A STAT3 palmitoylation cycle promotes T(H)17 differentiation and colitis. Nature *586*, 434–439. https://doi.org/10.1038/s41586-020-2799-2.

13. Kharbanda, A., Walter, D.M., Gudiel, A.A., Schek, N., Feldser, D.M., and Witze, E.S. (2020). Blocking EGFR palmitoylation suppresses PI3K signaling and mutant KRAS lung tumorigenesis. Sci. Signal. *13*, eaax2364. https://doi.org/10.1126/scisignal.aax2364.

14. Zhou, L., He, X., Wang, L., Wei, P., Cai, Z., Zhang, S., Jin, S., Zeng, H., and Cui, J. (2022). Palmitoylation restricts SQSTM1/p62-mediated autophagic degradation of NOD2 to modulate inflammation. Cell Death Differ. *29*, 1541–1551. https://doi.org/10.1038/s41418-022-00942-z.

15. Lu, Y., Zheng, Y., Coyaud, É., Zhang, C., Selvabaskaran, A., Yu, Y., Xu, Z., Weng, X., Chen, J.S., Meng, Y., et al. (2019). Palmitoylation of NOD1 and NOD2 is required for bacterial sensing. Science *366*, 460–467. https://doi.org/10.1126/science.aau6391.

16. Hao, J.W., Wang, J., Guo, H., Zhao, Y.Y., Sun, H.H., Li, Y.F., Lai, X.Y., Zhao, N., Wang, X., Xie, C., et al. (2020). CD36 facilitates fatty acid uptake by dynamic palmitoylation-regulated endocytosis. Nat. Commun. *11*, 4765. https://doi.org/10.1038/s41467-020-18565-8.

17. Bijlmakers, M.J., and Marsh, M. (2003). The on-off story of protein palmitoylation. Trends Cell Biol. *13*, 32–42. https://doi.org/10.1016/s0962-8924(02)00008-9.

18. Ren, W., Jhala, U.S., and Du, K. (2013). Proteomic analysis of protein palmitoylation in adipocytes. Adipocyte *2*, 17–28. https://doi.org/10.4161/adip.22117.

19. Pedram, A., Razandi, M., Deschenes, R.J., and Levin, E.R. (2012). DHHC-7 and -21 are palmitoylacyltransferases for sex steroid receptors. Mol. Biol. Cell *23*, 188–199. https://doi.org/10.1091/mbc.E11-07-0638.

20. van Houten, E.L.A.F., and Visser, J.A. (2014). Mouse models to study polycystic ovary syndrome: a possible link between metabolism and ovarian function? Reprod. Biol. *14*, 32–43. https://doi.org/10.1016/j.repbio.2013.09.007.

21. Hillier, S.G., and Tetsuka, M. (1997). Role of androgens in follicle maturation and atresia. Baillieres Clin. Obstet. Gynaecol. *11*, 249–260. https://doi.org/10.1016/s0950-3552(97)80036-3.

22. Sen, A., and Hammes, S.R. (2010). Granulosa cell-specific androgen receptors are critical regulators of ovarian development and function. Mol. Endocrinol. *24*, 1393–1403. https://doi.org/10.1210/me.2010-0006.

23. Walters, K.A., Allan, C.M., Jimenez, M., Lim, P.R., Davey, R.A., Zajac, J.D., Illingworth, P., and Handelsman, D.J. (2007). Female mice

haploinsufficient for an inactivated androgen receptor (AR) exhibit age-dependent defects that resemble the AR null phenotype of dysfunctional late follicle development, ovulation, and fertility. Endocrinology *148*, 3674–3684. https://doi.org/10.1210/en.2007-0248.

24. Gioeli, D., Black, B.E., Gordon, V., Spencer, A., Kesler, C.T., Eblen, S.T., Paschal, B.M., and Weber, M.J. (2006). Stress kinase signaling regulates androgen receptor phosphorylation, transcription, and localization. Mol. Endocrinol. *20*, 503–515. https://doi.org/10.1210/me.2005-0351.

25. Zuehlke, A.D., Beebe, K., Neckers, L., and Prince, T. (2015). Regulation and function of the human HSP90AA1 gene. Gene *570*, 8–16. https://doi.org/10.1016/j.gene.2015.06.018.

26. Lyly, A., von Schantz, C., Heine, C., Schmiedt, M.L., Sipilä, T., Jalanko, A., and Kyttälä, A. (2009). Novel interactions of CLN5 support molecular networking between Neuronal Ceroid Lipofuscinosis proteins. BMC Cell Biol. *10*, 83. https://doi.org/10.1186/1471-2121-10-83.

27. Davies, T.H., Ning, Y.M., and Sánchez, E.R. (2002). A new first step in activation of steroid receptors: hormone-induced switching of FKBP51 and FKBP52 immunophilins. J. Biol. Chem. *277*, 4597–4600. https://doi.org/10.1074/jbc.C100531200.

28. Sarkar, A.A., and Zohn, I.E. (2012). Hectd1 regulates intracellular localization and secretion of Hsp90 to control cellular behavior of the cranial mesenchyme. J. Cell Biol. *196*, 789–800. https://doi.org/10.1083/jcb.201105101.

29. Krzemień-Ojak, Ł., Góral, A., Joachimiak, E., Filipek, A., and Fabczak, H. (2017). Interaction of a novel chaperone PhLP2A with the heat shock protein Hsp90. J. Cell. Biochem. *118*, 420–429. https://doi.org/10.1002/jcb.25669.

30. Lindzey, J., Grossmann, M., Kumar, M.V., and Tindall, D.J. (1993). Regulation of the 5′-flanking region of the mouse androgen receptor gene by cAMP and androgen. Mol. Endocrinol. *7*, 1530–1540. https://doi.org/10.1210/mend.7.12.7511785.

31. Merkle, D., and Hoffmann, R. (2011). Roles of cAMP and cAMP-dependent protein kinase in the progression of prostate cancer: cross-talk with the androgen receptor. Cell. Signal. *23*, 507–515. https://doi.org/10.1016/j.cellsig.2010.08.017.

32. Qiao, J., and Feng, H.L. (2011). Extra- and intra-ovarian factors in polycystic ovary syndrome: impact on oocyte maturation and embryo developmental competence. Hum. Reprod. Update *17*, 17–33. https://doi.org/10.1093/humupd/dmq032.

33. Ciacciarelli, M., Zerbinati, C., Violi, F., and Iuliano, L. (2015). Dipyridamole: a drug with unrecognized antioxidant activity. Curr. Top. Med. Chem. *15*, 822–829. https://doi.org/10.2174/1568026615666150220111942.

34. (1995). Venous thromboembolic disease and combined oral contraceptives: results of international multicentre case-control study. World Health Organization Collaborative Study of Cardiovascular Disease and Steroid Hormone Contraception. Lancet *346*, 1575–1582.

35. Targher, G., Zoppini, G., Bonora, E., and Moghetti, P. (2014). Hemostatic and fibrinolytic abnormalities in polycystic ovary syndrome. Semin. Thromb. Hemost. *40*, 600–618. https://doi.org/10.1055/s-0034-1384512.

36. Wang, J., Wu, D., Guo, H., and Li, M. (2019). Hyperandrogenemia and insulin resistance: the chief culprit of polycystic ovary syndrome. Life Sci. *236*, 116940. https://doi.org/10.1016/j.lfs.2019.116940.

37. Li, S., Zhai, J., Chu, W., Geng, X., Chen, Z.J., and Du, Y. (2020). Altered circadian clock as a novel therapeutic target for constant darkness-induced insulin resistance and hyperandrogenism of polycystic ovary syndrome. Transl. Res. *219*, 13–29. https://doi.org/10.1016/j.trsl.2020.02.003.

38. Huang-Doran, I., Kinzer, A.B., Jimenez-Linan, M., Thackray, K., Harris, J., Adams, C.L., de Kerdanet, M., Stears, A., O'Rahilly, S., Savage, D.B., et al. (2021). Ovarian hyperandrogenism and response to gonadotropin-releasing hormone analogues in primary severe insulin resistance. J. Clin. Endocrinol. Metab. *106*, 2367–2383. https://doi.org/10.1210/clinem/dgab275.

39. Deyev, I.E., Popova, N.V., Serova, O.V., Zhenilo, S.V., Regoli, M., Bertelli, E., and Petrenko, A.G. (2017). Alkaline pH induces IRR-mediated phosphorylation of IRS-1 and actin cytoskeleton remodeling in a pancreatic beta cell line. Biochimie *138*, 62–69. https://doi.org/10.1016/j.biochi.2017.04.002.

40. Batishchev, O.V., Kuzmina, N.V., Mozhaev, A.A., Goryashchenko, A.S., Mileshina, E.D., Orsa, A.N., Bocharov, E.V., Deyev, I.E., and Petrenko, A.G. (2021). Activity-dependent conformational transitions of the insulin receptor-related receptor. J. Biol. Chem. *296*, 100534. https://doi.org/10.1016/j.jbc.2021.100534.

41. Shah, N.A., Antoine, H.J., Pall, M., Taylor, K.D., Azziz, R., and Goodarzi, M.O. (2008). Association of androgen receptor CAG repeat polymorphism and polycystic ovary syndrome. J. Clin. Endocrinol. Metab. *93*, 1939–1945. https://doi.org/10.1210/jc.2008-0038.

42. Peng, C.Y., Long, X.Y., and Lu, G.X. (2010). Association of AR rs6152G/A gene polymorphism with susceptibility to polycystic ovary syndrome in Chinese women. Reprod. Fertil. Dev. *22*, 881–885. https://doi.org/10.1071/rd09190.

43. Millson, S.H., Truman, A.W., Rácz, A., Hu, B., Panaretou, B., Nuttall, J., Mollapour, M., Söti, C., and Piper, P.W. (2007). Expressed as the sole Hsp90 of yeast, the alpha and beta isoforms of human Hsp90 differ with regard to their capacities for activation of certain client proteins, whereas only Hsp90beta generates sensitivity to the Hsp90 inhibitor radicicol. FEBS J. *274*, 4453–4463. https://doi.org/10.1111/j.1742-4658.2007.05974.x.

44. Li, L., Chen, N., Xia, D., Xu, S., Dai, W., Tong, Y., Wang, L., Jiang, Z., You, Q., and Xu, X. (2021). Discovery of a covalent inhibitor of heat shock protein 90 with antitumor activity that blocks the co-chaperone binding via C-terminal modification. Cell Chem. Biol. *28*, 1446–1459.e6. https://doi.org/10.1016/j.chembiol.2021.03.016.

45. Lees-Miller, S.P., and Anderson, C.W. (1989). The human double-stranded DNA-activated protein kinase phosphorylates the 90-kDa heat-shock protein, hsp90 alpha at two NH2-terminal threonine residues. J. Biol. Chem. *264*, 17275–17280.

46. Lees-Miller, S.P., and Anderson, C.W. (1989). Two human 90-kDa heat shock proteins are phosphorylated in vivo at conserved serines that are phosphorylated in vitro by casein kinase II. J. Biol. Chem. *264*, 2431–2437.

47. Martínez-Ruiz, A., Villanueva, L., González de Orduña, C., López-Ferrer, D., Higueras, M.A., Tarín, C., Rodríguez-Crespo, I., Vázquez, J., and Lamas, S. (2005). S-nitrosylation of Hsp90 promotes the inhibition of its ATPase and endothelial nitric oxide synthase regulatory activities. Proc. Natl. Acad. Sci. USA *102*, 8525–8530. https://doi.org/10.1073/pnas.0407294102.

48. Kaku, N., Matsuda, K.i., Tsujimura, A., and Kawata, M. (2008). Characterization of nuclear import of the domain-specific androgen receptor in association with the importin alpha/beta and Ran-guanosine 5′-triphosphate systems. Endocrinology *149*, 3960–3969. https://doi.org/10.1210/en.2008-0137.

49. Schopf, F.H., Biebl, M.M., and Buchner, J. (2017). The HSP90 chaperone machinery. Nat. Rev. Mol. Cell Biol. *18*, 345–360. https://doi.org/10.1038/nrm.2017.20.

50. Moilanen, A.M., Poukka, H., Karvonen, U., Häkli, M., Jänne, O.A., and Palvimo, J.J. (1998). Identification of a novel RING finger protein as a coregulator in steroid receptor-mediated gene transcription. Mol. Cell Biol. *18*, 5128–5139. https://doi.org/10.1128/mcb.18.9.5128.

51. Huang, B., Chen, Z., Geng, L., Wang, J., Liang, H., Cao, Y., Chen, H., Huang, W., Su, M., Wang, H., et al. (2019). Mucosal profiling of pediatric-onset colitis and IBD reveals common pathogenics and therapeutic pathways. Cell. *179*, 1160–1176.e24. https://doi.org/10.1016/j.cell.2019.10.027.

52. McLean, A.C., Valenzuela, N., Fai, S., and Bennett, S.A. (2012). Performing vaginal lavage, crystal violet staining, and vaginal cytological evaluation for mouse estrous cycle staging identification. J. Vis. Exp. e4389. https://doi.org/10.3791/4389.

53. Qi, X., Yun, C., Sun, L., Xia, J., Wu, Q., Wang, Y., Wang, L., Zhang, Y., Liang, X., Wang, L., et al. (2019). Gut microbiota-bile acid-interleukin-22 axis orchestrates polycystic ovary syndrome. Nat. Med. *25*,

1225–1233. https://doi.org/10.1038/s41591-019-0509-0.

54. Ge, X., He, Z., Cao, C., Xue, T., Jing, J., Ma, R., Zhao, W., Liu, L., Jueraitetibaike, K., Ma, J., et al. (2022). Protein palmitoylation-mediated palmitic acid sensing causes blood-testis barrier damage via inducing ER stress. Redox Biol. *54*, 102380. https://doi.org/10.1016/j.redox.2022.102380.

55. Wegleiter, T., Buthey, K., Gonzalez-Bohorquez, D., Hruzova, M., Bin Imtiaz, M.K., Abegg, A., Mebert, I., Molteni, A., Kollegger, D., Pelczar, P., and Jessberger, S. (2019). Palmitoylation of BMPR1a regulates neural stem cell fate. Proc. Natl. Acad. Sci. USA *116*, 25688–25696. https://doi.org/10.1073/pnas.1912671116.

56. Wan, J., Roth, A.F., Bailey, A.O., and Davis, N.G. (2007). Palmitoylated proteins: purification and identification. Nat. Protoc. *2*, 1573–1584. https://doi.org/10.1038/nprot.2007.225.

57. Brigidi, G.S., and Bamji, S.X. (2013). Detection of protein palmitoylation in cultured hippocampal neurons by immunoprecipitation and acyl-biotin exchange (ABE). J. Vis. Exp. *72*, 50031. https://doi.org/10.3791/50031.

STAR★METHODS

KEY RESOURCES TABLE

REAGENT or RESOURCE	SOURCE	IDENTIFIER
Antibodies		
Rabbit anti-HSP90α polyclonal antibody	Proteintech	Cat# 13171-1-AP, RRID: AB_2120924
Rabbit anti-PPT1 polyclonal antibody	Proteintech	Cat# 10887-1-AP, RRID: AB_2168906
Rabbit anti-LAMP1 monoclonal antibody	Abcam	Cat#ab208943, RRID: AB_2923327
Mouse anti-DYDDDDK Tag monoclonal antibody	Proteintech	Cat# 66008-3-Ig, RRID: AB_2749837
Mouse anti-GAPDH monoclonal antibody	Proteintech	Cat# 60004-1-Ig, RRID: AB_2107436
Mouse anti-beta actin monoclonal antibody	Proteintech	Cat#66009-1-Ig, RRID: AB_2687938
Rabbit anti-HA tag polyclonal antibody	Proteintech	Cat#51064-2-AP, RRID: AB_11042321
Mouse anti-Vinculin monoclonal antibody	Proteintech	Cat#66305-1-Ig, RRID: AB_2810300
Goat anti-Mouse IgG (H+L) Secondary Antibody, HRP	Thermo Fisher Scientific	Cat#31430, RRID: AB_228307
Goat anti-Rabbit IgG (H+L) Secondary Antibody, HRP	Thermo Fisher Scientific	Cat#31460, RRID: AB_228341
HRP-labeled Streptavidin	Beyotime	Cat#A0303, RRID: AB_2933973
Bacterial and virus strains		
Escherichia coli DH5a	TIANGEN	Cat#CB101
Escherichia coli TOP10	TIANGEN	Cat#CB104
Biological samples		
paraffin-embedded specimens from patients	Jinling Hospital of Nanjing Medical University; Women's Hospital of Nanjing Medical University	N/A
Chemicals, peptides, and recombinant proteins		
Dehydroepiandrosterone	Sigma-Aldrich	Cat#D4000
Dipyridamole	Sigma-Aldrich	Cat#9766
Corn oil	Sigma-Aldrich	Cat#C8267
Penicillin/streptomycin	Gibco	Cat#15140-122
Normocin	InvivoGen	Cat#ant-nr-1
PMSG	Ningbo 2nd Hormone Factory	N/A
hCG	Ningbo 2nd Hormone Factory	N/A
Hyaluronidase	Sigma-Aldrich	Cat#H3884
Protease inhibitor cocktail	Roche	Cat#4693116001
Phosphatase inhibitor cocktails	Roche	Cat#04906837001
NEM	Sigma-Aldrich	Cat#E3876
Biotin-BMCC	Thermo Fisher Scientific	Cat#21900
HPDP-Biotin	Thermo Fisher Scientific	Cat#21341
DHT	Sigma-Aldrich	Cat#D-073
Trypsin, sequencing grade	Promega	Cat#V5280
Tris, mass spectrometry grade	Sigma-Aldrich	Cat#T1503
SDS, mass spectrometry grade	Bio-Rad	Cat#1610302
DTT, mass spectrometry grade	Bio-Rad	Cat#1610610
Iodoacetamide, mass spectrometry grade	Bio-Rad	Cat#1632109
Formic acid, mass spectrometry grade	Thermo Fisher Scientific	Cat#85178
Acetonirile, mass spectrometry grade	Sigma-Aldrich	Cat#34851

(*Continued on next page*)

Continued

REAGENT or RESOURCE	SOURCE	IDENTIFIER
Critical commercial assays		
Mouse oestradiol ELISA kit	Mlbio	Cat#ml001962
Mouse testosterone ELISA kit	Mlbio	Cat#ml001948
Mouse LH ELISA kit	Cloud-clone	Cat#CEA441Mu
Mouse FSH ELISA kit	Cloud-clone	Cat#CEA830Mu
Mouse estrone ELISA kit	Mlbio	Cat#ml266215
Mouse androgen ELISA kit	Mlbio	Cat#ml001954
BCA Protein Assay Kit	Thermo Fisher Scientific	Cat#23225
Muta-Direct Kit	SBS Genetech	Cat#SDM-15
Luciferase assay system	Beyotime	Cat#RG027
Total RNA Purification Kit	EZBioscience	Cat#B0004-plus
HiScript III RT SuperMix	Vazyme	Cat#R312-01
SYBR qPCR Master Mix	Vazyme	Cat#Q111-02
Lysosome isolation Kit for mammalian Cells/Tissues	Invent	Cat#LY-034
Experimental models: Cell lines		
LNCaP clone FGC	ATCC	Cat# CRL-1740
HEK293T	ATCC	Cat#CRL-3216
KGN	BIUEFBIO	Cat#BFN60805961
GRM02	BIUEFBIO	Cat#BFN60810498
Experimental models: Organisms/strains		
Mouse: ICR strain	Jiangsu ALF Biotechnology Company	N/A
Oligonucleotides		
qPCR primers for mouse *Cyp19a1*: forward: 5′-AACCCCATGCAGTATAATGTCAC-3′ reverse: 5′-AGGACCTGGTATTGAAGACGAG-3′	Harvard Primer Bank	156139071c1
qPCR primers for mouse *Gapdh*: forward: 5′- AGGTCGGTGTGAACGGATTTG-3′ reverse: 5′-TGTAGACCATGTAGTTGAGGTCA-3′	Harvard Primer Bank	126012538c1
qPCR primers for human *CYP19A1*: forward: 5′-TCCTATCAGGACGGAAGGTCC-3′ reverse: 5′-GTTCCTTGACCTCAGAGGGG-3′	This paper	N/A
qPCR primers for mouse *GAPDH*: forward: 5′-GGGAAGCTTGTCATCAATGGAA-3′ reverse: 5′-AGAGATGATGACCCTTTTGGCTC-3′	This paper	N/A
Recombinant DNA		
pcDNA3.1-3×Flag-*m*Hsp90αα1-WT	This paper	N/A
pcDNA3.1-3×Flag-*m*Hsp90αα1-C598S	This paper	N/A
pcDNA3.1-3×Flag-*m*Hsp90αα1-C599S	This paper	N/A
pcDNA3.1-3×Flag-*m*Hsp90αα1-C598,599S	This paper	N/A
pcDNA3.1-3×Flag-*h*Hsp90αα1-WT	This paper	N/A
pcDNA3.1-3×Flag-*h*Hsp90αα1-C597,598S	This paper	N/A
pcDNA3.1-3×HA-*m*LYPLA1	This paper	N/A
pcDNA3.1-3×HA-*m*LYPLA2	This paper	N/A
pcDNA3.1-3×HA-*m*ABHD17A	This paper	N/A
pcDNA3.1-3×HA-*m*ABHD17B	This paper	N/A

(*Continued on next page*)

Continued

REAGENT or RESOURCE	SOURCE	IDENTIFIER
pcDNA3.1-3×HA-*m*ABHD17C	This paper	N/A
pcDNA3.1-3×HA-*m*PPT1	This paper	N/A
pARE2-TATA-Luc	Moilanen et al., 1998[50]	N/A
Software and algorithms		
ImageCal version1.10	Tanon	http://www.biotanon.com
Prism 8.0	GraphPad	http://www.graphpad.com
SPSS version 21.0	IBM	https://www.ibm.com/cn-zh/analytics/spss-statistics-software
ImageJ	NIH	https://imagej.nih.gov/ij
The mass spectrometry proteomics data	Proteome Xchange Consortium (http://proteomecentral.proteomexchange.org)	The dataset identifier: PXD028835
Other		
FuturePAGE™ 4–20% 12 wells	ACE Biotechnology	Cat#ET12420GEL
FuturePAGE™ 4–20% 15 wells	ACE Biotechnology	Cat#ET15420GEL
WB & IP lysis buffer	Beyotime	Cat# P0013
RIPA lysis buffer	Sigma-Aldrich	Cat#R0278
Protein A/G beads	Thermo Fisher Scientific	Cat#88847
Anti-Flag beads	Sigma-Aldrich	Cat#M8823
Streptavidin agarose resin	Thermo Fisher Scientific	Cat#20347
DMEM	Gibco	Cat#11995020
RPMI-1640	Gibco	Cat#61870036
Opti-MEM	Gibco	Cat#31980070
DMEM-F12	BasalMedia	Cat#L310KJ
FBS	Gibco	Cat#A3161002C
Lipofectamine 3000	Invitrogen	Cat#L3000015
PBS	GENOM	Cat#GNM10010
M2 medium	Sigma-Aldrich	Cat#M7167
2 × SDS loading buffer	FDbio	Cat#FD003
5 × SDS loading buffer	FDbio	Cat#FD002
PVDF membrane	Bio-Rad	Cat#1620177
Western antibody diluent	NCMbiotech	Cat#WB500D

RESOURCE AVAILABILITY

Lead contact

Further information and requests for resources and reagents should be directed to and will be fulfilled by the Lead Contact Bing Yao (yaobing@nju.edu.cn).

Materials availability

This study did not generate unique reagents.

Data and code availability

- The mass spectrometry proteomics data have been deposited in the ProteomeXchange Consortium via the PRIDE partner repository and are publicly available as of the date of publication. Accession number is listed in the key resources table.
- This article does not report original code.

- Any additional information required to reanalyze the data reported in this work paper is available from the lead contact upon request.

EXPERIMENTAL MODEL AND SUBJECT DETAILS

Mice

Female prepubertal (21 days old) mice of the ICR strain (Jiangsu ALF Biotechnology Company, Jiangsu, China) were randomly divided into different groups, housed 5–7 per cage, and maintained under controlled temperature (20–26°C), humidity (40–70%) and lighting (lights on at 08:00 a.m. and off 08:00 p.m.) conditions and standard laboratory conditions with free access to rodent feed and water. The animal experiments were approved by the Animal Research Committee of the Animal Care and Use Committee of Nanjing Medical University and were performed in accordance with established guidelines.

Cell lines

Human HEK293T cells (obtained from ATCC) and human GCs of the KGN line (obtained from BIUEFBIO) were grown in Dulbecco's minimal Eagle medium (DMEM, 11,965-092; Gibco, Grand Island, NY, USA), the human prostate cancer cell line (LNCaP clone FGC, obtained from ATCC) was cultured in RPMI-1640 (61870036; Gibco), and mouse GCs of the GRM02 line (obtained from BIUEFBIO) were maintained in DMEM/F12 (1:1) medium (L310KJ; BasalMedia, Shanghai, China) supplemented with 10% (vol/vol) foetal bovine serum (FBS, A3161002C; Gibco), 1% (vol/vol) penicillin/streptomycin (15140-122; Gibco) and 2% normocin (ant-nr-1; InvivoGen, San Diego, CA, USA) at 37°C in 5% CO_2 with 100% humidity.

Isolation of primary mouse granulosa cells

Female ICR mice were intraperitoneally injected (i.p.) with 10 IU pregnant mare serum gonadotropin (PMSG) (Ningbo 2nd Hormone Factory, Zhejiang, China) to stimulate follicular growth after DHEA-induced or control treatment for 21 days. After priming with PMSG for 48h, the mice were administered (i.p.) Human chorionic gonadotropin (hCG) (Ningbo 2nd Hormone Factory, 10 IU/mouse) was administered to stimulate follicular maturation. After 16h, the animals were sacrificed by cervical dislocation, and oviductal ampullae were washed with ice-cold phosphate-buffered saline (PBS) without Ca^{2+} and Mg^{2+} (GNM10010; GENOM, Shanghai, China) to remove blood. Cumulus-oocyte complexes were obtained by manually rupturing ovarian follicles with needle puncture under a stereoscopic microscope (SZM1000; Nikon, Japan). To collect primary GCs, cumulus-oocyte complexes were treated with hyaluronidase (H3884; Sigma-Aldrich, USA) for 30 s. Digestion was stopped with M2 medium (M7167; Sigma-Aldrich). Oocytes were removed by mouth pipetting under a stereoscopic microscope (SZM1000; Nikon), and then, primary GCs were collected to determine the *S*-palmitoylation levels of total protein.

METHOD DETAILS

The dehydroepiandrosterone (DHEA)-induced hyperandrogenism phenotype mouse model

The DHEA-induced hyperandrogenism phenotype mouse model was established based on a previous report.[20] Mice were subcutaneously injected (s.c.) with DHEA dissolved in sesame oil for the experimental groups (D4000; Sigma-Aldrich, USA; 60 mg/kg body weight per day for 21 days; both DHEA-induced groups and DHEA+DIP groups) or s.c. with sesame oil (control groups) for 21 days. After DHEA-induced treatment, mice were intragastrically injected (i.g.) with dipyridamole (D9766, Sigma-Aldrich, 50 mg/kg body weight) or vehicle (2% DMSO, 10% ethanol, 88% corn oil) every day for eight days. The dipyridamole treatment was based on a previous dipyridamole animal study.[51] The mice were anesthetized with ether and killed by cervical dislocation. Serum was collected to measure sex hormone levels at dioestrus stages. The ovaries were processed for haematoxylin and eosin staining. The remaining ovaries were quickly frozen and stored at −80°C. For haematoxylin-eosin (H&E) staining, ovaries were fixed in 4% paraformaldehyde (PFA) for 24h and embedded in paraffin. Sections (3 μm) were prepared and dewaxed prior to straining. The sera were collected for hormone level analysis; ovarian tissues were collected for H&E staining and immunohistochemistry (IHC); and primary granulosa cells were collected for acyl-biotin exchange (ABE) assay and WB.

Vaginal smears and oestrous cycle determination

Vaginal smears were taken daily at 5:00 p.m. from the 1st to the 10th day after the first day of dipyridamole treatment. The stage of the oestrous cycle was determined by microscopic analysis of the predominant cell

type in vaginal smears following H&E staining. Proestrus consists of round, nucleated epithelial cells; oestrus consists of cornified squamous epithelial cells; metestrus consists of epithelial cells and leukocytes; and dioestrus consists of nucleated epithelial cells and a predominance of leukocytes. The oestrous cycle was determined by classic criteria, as previously described.[52]

Serum analysis

Blood samples were collected in 1.5 mL EP tubes, blood clotting was performed for 1h at 4°C, and the tubes were centrifuged at 500 × *g*/4°C for 10 min to harvest serum. Serum samples and conditional cell culture media were stored at −80°C for subsequent serum determinations. The levels of oestradiol (E2) (ml001962; mlbio, Shanghai, China), testosterone (ml001948; mlbio), luteinizing hormone (CEA441Mu; Cloud-Clone, Wuhan, Hubei, China), follicle-stimulating hormone (CEA830Mu; Cloud-Clone), estrone (E1) (ml266215; mlbio) and androgen (ml001954; mlbio) were determined by enzyme-linked immunosorbent assay kits for mice.

Human tissue specimens

Paraffin-embedded specimens from patients with ovarian hyperandrogenism in PCOS were obtained surgically and were obtained from Jinling Hospital of Nanjing Medical University. Women with PCOS were diagnosed according to the 2003 Rotterdam criteria, which require the presence of at least two of the following: (1) oligo-ovulation and/or anovulation; (2) clinical and/or biochemical signs of hyperandrogenism; and (3) polycystic ovaries. We collected five paraffin-embedded ovarian tissues from patients with PCOS who performed bilateral ovarian wedge resection (OWR) to induce ovulation surgically in the Department of Obstetrics and Gynecology at Jinling Hospital of Nanjing University. Comparative control samples were tissues of surgical patients (including two cases were mucinous cystadenoma, one case was serous cystadenoma and two cases were endometrial cyst) without ovarian hyperandrogenism from Women's Hospital of Nanjing Medical University. Written informed consent was obtained from all participants Collection of all samples was approved by the local ethical committee and the institutional review board of Women's Hospital of Nanjing Medical University. Each patient gave written informed consent, and patient data were anonymized. Detailed information on the patients is included in Table S3.

Morphology and immunohistochemistry

Paraffin-embedded sections of ovarian tissues were processed as reported previously.[53] Ovaries were quickly collected, fixed in 4% PFA, placed in 75% ethanol, dehydrated, and embedded in paraffin. Paraffin blocks were longitudinally and serially cut into 3 μm sections (HM 325; Thermo, USA) and stained with H&E or used for IHC staining. Primary antibodies used to stain the sections included rabbit anti-mouse HSP90α (Proteintech Cat# 13171-1-AP, RRID: AB_2120924, dilution ration: 1:200), rabbit anti-human PPT1 (Proteintech Cat# 10887-1-AP, RRID: AB_2168906, dilution ration: 1:100). Morphology and IHC images were acquired with a light upright microscope (NIS-Elements 3.2; ECLIPSE 80i; Nikon, Japan). The numbers of corpora lutea and cystic follicles were counted. The results were confirmed by a pathologist.

Acyl-biotin exchange (ABE)-based sample preparation for mass spectrometry

Enrichment of S-palmitoylated proteins by ABE

Tissue lysis and downstream sample preparation for mass spectrometry analysis of *S*-palmitoylated proteins were carried out as previously described.[54,55] Ovarian tissues collected from the DHEA-induced ovarian hyperandrogenism group (DHEA group) (n=9) or control group (n=9) were divided into three tubes as repeats. Based on the protein level from mouse tissues, each tube contained three pairs of ovaries for *S*-palmitoylated protein enrichment. Each of DHEA group and control group ovarian tissues was lysed in RIPA buffer (R0278; Sigma-Aldrich) containing 1 mM PMSF (Beyotime, Shanghai, China) and protease inhibitor cocktails (04906837001; Roche) by grinding (60 Hz, 30s) with high-speed low temperature tissue grinding machine (KZ-III-F, Servicebio, Wubei, China). This process was repeat four times. After centrifugation at 12,000 *g*/4°C for 10 min, the protein-containing supernatant was collected and measured by BCA assay (Thermo Scientific). Samples were adjusted to the same volume and concentration (1 mL and 2 mg/mL, respectively) by the addition of lysis buffer. Protein was irreversible blockaded of unmodified cysteine thiol groups with N-ethylmaliemide (NEM, Sigma-Aldrich, 50 mM, 4°C in the dark, overnight). After precipitation with methanol/chloroform, the protein samples were diluted in 200 μL resuspension buffer (4% SDS, 50 mM Tris and 5 mM EDTA, pH 7.4), and each sample was split into two equal parts (100 μL per part): plus-hydroxylamine (HAM, Sigma-Aldrich) (+HAM sample) and minus-HAM (-HAM sample). +HAM sample was mixed with 800 μL 1 M HAM, 1 mM EDTA, protease inhibitors and 100 μL 4 mM HPDP-Biotin (Thermo Scientific).

The negative control group (-HAM sample) was treated identically but HAM was replaced by 50 mM Tris (pH 7.4). Samples were incubated at room temperature in the dark with rotating for 2 h. Samples were precipitated again and dissolved in 100 μL of resuspension buffer, and added with 900 μL PBS containing 0.2% Triton X-100 and 15 μL streptavidin-coated beads (Thermo Scientific) with shaking overnight at 4°C. Beads were washed five times with PBS. Finally, the beads were mixed with 2 × SDS loading buffer and boiled at 95°C for 5 min.

LC-MS/MS for the proteomic study

For liquid chromatography (LC)–MS/MS analysis, the protocol was performed as previously described.[56] Briefly, palmitoylated proteins (100 μg) extracted and purified from each sample were reduced by dithiothreitol (DTT, 1610404; Bio-Rad) and alkylated by iodoacetamide (IAA, 1632109; Bio-Rad). After digest with trypsin (V5280; Promega, an enzyme-to-substrate ratio of 1:20, 37°C, 4h), the peptide mixtures were desalted by ultrafiltration tube, freeze dried and then dissolved in mobile phase A buffer (2% acetonitrile, 0.1% formic acid). After centrifugation at 20,000 *g* for 10 min, the supernatant was loaded on UltiMate 3000 UHPLC (Thermo Scientific) for separation and subjected to trap column for enrichment and desalting. The peptides of each sample were fractionated with a 75 μm * 25 cm C18 analytical column (3 μm beads) and separated with a linear gradient (5–80%) of mobile phase B buffer (98% acetonitrile, 0.1% formic acid). The flow rate was set at 300 nL/min. Peptides were eluted from the column and nanosprayed directly into a tandem mass spectrometer Q-Exactive HF-X (Thermo Scientific) for a data dependent acquisition (DDA) mode operation. The main parameters were set as follows: ion source voltage – 1.9 kV, MS1 resolution – 60,000, mass range – 350 to 1,500 m/z. MS2 initial mass range fixed at 100 m/z, resolution – 15,000. The parent ion screen conditions for MS2 were charge state include 2+ to 6+, and the top 30% parent ion with the peak intensity exceeding 10,000. The ion fragmentation was detected in Orbitrap with a high-energy collision dissociation activation energy (HCD) mode. Additional parameters were as follows: dynamic exclusion: 30 s, automated gain control (AGC) target: 3.0e6 (MS1) and 1.0e5 (MS2). The MS raw data were analysed by Max Quant (Version: 1.5.3.30; Max Planck Institutes) integrated Andromeda engine using a combination of the UniProt *Mus musculus* protein database (17,006 sequences). The analysis was performed by Huada Gene Research Institute (Shenzhen, China).

Cloning and mutagenesis

Mouse Hsp90αα1 (*m*Hsp90αα1) cDNA (Gene ID: 15519), human HSP90AA1 (*h*HSP90AA1) cDNA (Gene ID: 3320), *m*LYPLA1, *m*LYPLA2, *m*ABHD17A, *m*ABHD17B, *m*ABHD17C and *m*PPT1 were synthesized by Gene Create (Wuhan, China) and subcloned into the pcDNA3.1 (+)-vector with Flag or hemagglutinin (3×HA). The luciferase reporter vector pARE2-TATA-Luc was purchased from Gene Create (Wuhan, China).[50] Mutants for *m*Hsp90αα1 and *h*HSP90AA1 were generated with a two-step PCR strategy and overlapping primers using a Muta-Direct Kit (SDM-15; SBS Genetech, Beijing, China), and the sequence was verified by Sanger sequencing (GENEWIZ, Suzhou, China). The primers for the mutant-type allele were as follows:

*m*Hsp90αα1^{C598S} forward: 5′-CTGGTGACATCCCCGAGCTGTATTGTCACA-3′;

*m*Hsp90αα1^{C598S} reverse: 5′-TGTGACAATACAGCTCGGGGATGTCACCAG-3′;

*m*Hsp90αα1^{C599S} forward: 5′-TGACATCCCCGTGCTCTATTGTCACAAGCA-3′;

*m*Hsp90αα1^{C599S} reverse: 5′-TGCTTGTGACAATAGAGCACGGGGATGTCA-3′;

*m*Hsp90αα1$^{C598,\ 599S}$ forward: 5′-CTGGTGACATCCCCGAGCAGTATTGTCACA-3′;

*m*Hsp90αα1$^{C598,\ 599S}$ reverse: 5′-TGTGACAATACTGCTCGGGGATGTCACCAG-3′;

*h*HSP90AA1$^{C597,\ 598S}$ forward: 5′- GTGACATCTCCAAGCAGTATTGTCACAAGC-3′; and

*h*HSP90AA1$^{C597,\ 598S}$ forward: 5′- GCTTGTGACAATACTGCTTGGAGATGTCAC-3′.

Immunoprecipitation analysis

Whole-cell extracts were prepared after transfection, followed by incubation overnight with the appropriate antibodies plus Protein A/G beads (88,847; Thermo Scientific). For immunoprecipitation with

anti-Flag, anti-Flag M2 magnetic beads (M8823; Sigma-Aldrich) were incubated with whole cell extracts. After five rinses with lysis buffer (P0013; Beyotime), immunoprecipitates were eluted with 2 × SDS loading buffer (FD003; FDbio, Zhejiang, China) and resolved by SDS-PAGE. Proteins were transferred to polyvinylidene fluoride (PVDF) membranes (1620177; Bio-Rad, USA) and blocked in Western blocking buffer (P0252; Beyotime). Appropriate antibodies were applied in Western antibody diluent (WB500D; NCMbiotech, Suzhou, China) overnight at 4°C.

Immunoblot analysis

Cells and ovarian tissue samples were lysed with lysis buffer (P0013; Beyotime) with protease inhibitor cocktails (04906837001; Roche, Mannheim, Germany) and phosphatase inhibitor cocktails (04906837001; Roche). Cell samples were lysed on ice for 30 min with gentle rocking, and tissue samples were lysed with ultrasound treatment by a high-speed tissue grinding machine. After centrifugation at 12,000 *g*/4°C for 10 min, the supernatants were harvested and stored at −80°C until further use. Protein concentrations were determined by using a BCA kit (23225; Thermo Scientific) according to the manufacturer's protocols. For immunoblot analysis, lysates were boiled at 100°C for 10 min in 5 × SDS loading buffer (FD002; FDbio) and resolved by SDS-PAGE. Protein was transferred onto PVDF membranes and blocked in Western blocking buffer. Appropriate antibodies were applied in Western antibody diluent (WB500D; NCMbiotech) overnight at 4°C. Immobilon Western Chemiluminescent HRP Substrate (BL520A; Biosharp) was used for protein detection. Images were obtained using a chemiluminescence imaging analysis system (5200; Tanon, Shanghai, China) and ImageCal version 1.10 (Tanon).

Acyl-biotin exchange (ABE) assay

The ABE assay was performed as previously described with minor modifications.[57] HEK293T cells transiently expressing Flag-tagged *m*HSP90α together with 3×HA-tagged de-palmitoylation family members (*m*LYPLA1, *m*LYPLA2, *m*ABHD17A, *m*ABHD17B, *m*ABHD17C, and *m*PPT1) were harvested 48h after transfection and rinsed with cold PBS. Cells were collected in 50 mM *N*-ethylmaleimide (NEM) (E3876; Sigma-Aldrich) containing lysis buffer (50 mM Tris-HCl pH 7.5, 150 mM NaCl, 1 mM $MgCl_2$, 1% NP-40, 10% glycerol, protease inhibitor and phosphatase inhibitor), incubated on a rocker with ice for 30 min, and then rotationally incubated for 1.5h at 4°C. Cell lysates were centrifuged at 12,000 × *g*/4°C for 10 min, and the supernatants were incubated with anti-Flag beads (M8823; Sigma-Aldrich) at 4°C for 3h. After incubation, the beads were rinsed five times with lysis buffer at pH 7.5 and then three times with lysis buffer at pH 7.2. After incubation with freshly prepared hydroxylamine (HAM)-containing lysis buffer (50 mM Tris-HCl pH 7.5, 150 mM NaCl, 1 mM $MgCl_2$, 1% NP-40, 10% glycerol, protease inhibitor and phosphatase inhibitor) at room temperature for 1h with gentle rotation, beads were rinsed five times with lysis buffer at pH 7.2 and three times with lysis buffer at pH 6.2. After washing with lysis buffer to remove unbound HAM, beads were resuspended in 5 μM biotin-BMCC (21900; Thermo Scientific) in lysis buffer (pH 6.2) at 4°C for 1h and rinsed once with lysis buffer (pH 6.2). Subsequently, beads were boiled at 98°C for 10 min in 2 × SDS loading buffer and analysed by Western blot using DYDDDDK Tag monoclonal antibody (Proteintech Cat# 66008-3-Ig, RRID: AB_2749837, dilution ratio: 1:3000) and HRP-labelled streptavidin (A0303; Beyotime; dilution ratio: 1:5000). The ovaries and primary granulocytes are shown in Figure 1B, according to a protocol adapted from a previous report.[56]

Luciferase assay

HEK293T cells were seeded in 24-well plates and transfected using Lipofectamine 3000 with pARE2-TATA-Luc (firefly luciferase; 100 ng) and pRL-TK (Renilla luciferase plasmid; 10 ng) together with 500 ng plasmids encoding *m*Hsp90αα1 or *m*Hsp90αα1^{C598,599S}. After 4h, the cells were stimulated with DHT (D-073; Sigma-Aldrich) dissolved in methanol (100 nM for experimental groups) or with methanol (for control groups) for 24h. Cells were harvested, and the luciferase assay was performed using the Luciferase Assay System (RG027; Beyotime) with a Luminoskan Ascent luminometer (BK-96-C; BIOSNO) according to the manufacturer's protocol. Reporter gene activity was determined by normalization of firefly luciferase activity to Renilla luciferase activity.

RNA extraction and quantitative RT-qPCR

Total RNA was extracted using a Total RNA Purification Kit (B0004-plus; EZBioscience, Suzhou, China), and cDNA was reverse-transcribed from 1 μg total RNA using HiScript III RT SuperMix (R312-01; Vazyme, Nanjing, China) according to the manufacturer's protocol. RT-qPCR was performed in triplicate in 96-well plates

using SYBR qPCR Master Mix (Q111-02; Vazyme) with gene-specific forward and reverse primers. cDNA was amplified for 40 cycles using a Roche LC480 Real-time PCR system. *Gapdh* or *GAPDH* was used as a reference gene.

For comparisons, mRNA expression levels were normalized to those of the blank/culture medium treatment condition for each subject. The primers were as follows:

Mouse *Cyp19a1* forward: 5′-AACCCCATGCAGTATAATGTCAC-3′;

Mouse *Cyp19a1* reverse: 5′-AGGACCTGGTATTGAAGACGAG-3′;

Mouse *Gapdh* forward: 5′- AGGTCGGTGTGAACGGATTTG-3′;

Mouse *Gapdh* reverse: 5′-TGTAGACCATGTAGTTGAGGTCA-3′;

Human *CYP19A1* forward: 5′-TCCTATCAGGACGGAAGGTCC-3′;

Human *CYP19A1* forward: 5′-GTTCCTTGACCTCAGAGGGG-3′;

Human *GAPDH* forward: 5′-GGGAAGCTTGTCATCAATGGAA-3′; and

Human *GAPDH* reverse: 5′-AGAGATGATGACCCTTTTGGCTC-3′.

Lysosome isolation assay

HEK293T cells from five 10 cm culture dishes (85% confluence) were washed once with cold PBS (5 mL per dish) and harvested using a cell scraper. Collected cells by centrifugation (500 × *g*, 5 min). To evaluate the distribution of HSP90α in lysosome fractions, lysosomes were purified by a commercial lysosome isolation kit for mammalian cells (LY-034; Invent, Beijing, China) according to the manufacturer's instructions. All buffers used for lysosome isolation contained protease inhibitor (04906837001; Roche) and all centrifugation steps were performed at 4°C. The insoluble lysosome fractions were dissolved in WB lysis buffer (P0013, Beyotime) for immunoblot assay. The purity of the prepared lysosomes from HEK293T cells was determined by immunoblot measuring lysosomal associated membrane protein 1 (LAMP1; Abcam Cat# ab208943, RRID: AB_2923327, dilution ratio: 1:1000) expression.

QUANTIFICATION AND STATISTICAL ANALYSIS

For the experimental data, statistical analyses and graphics production were performed using GraphPad Prism 8 and SPSS version 21.0. Detailed descriptions of the statistical tests are specified in the Results section and in the Figure Legends.